TP53-mediated clonal hematopoiesis confers increased risk for incident peripheral artery disease

Seyedeh M. Zekavat BS[1-4]*, Vanesa Viana-Huete PhD[5]*, María A. Zuriaga PhD[5], Md Mesbah Uddin PhD[3,4], Mark Trinder BS[3,4,6], Kaavya Paruchuri MD[3,4,7], Nuria Matesanz PhD[5], Virginia Zorita BS MSc[5], Alba Ferrer-Pérez BS MSc[5], Marta Amorós-Pérez BS MSc[5], Scott M. Damrauer MD[8], Christie M. Ballantyne MD[9], Abhishek Niroula PhD[3,10], Christopher J. Gibson MD[10], James Pirruccello MD[3], Gabriel Griffin MD[11], Benjamin L. Ebert MD PhD[12], Peter Libby MD PhD[7], Valentín Fuster MD PhD[5,13], Hongyu Zhao PhD[14], Pradeep Natarajan MD MMSc[3,4,7§], Alexander G. Bick MD PhD[3,15§], José J Fuster PhD[5,16§], Derek Klarin MD[3,17,18§]

1. Yale School of Medicine, New Haven, CT;
2. Computational Biology & Bioinformatics Program, Yale University, New Haven, CT, USA;
3. Program in Medical and Population Genetics, Broad Institute of MIT and Harvard, Cambridge, MA, USA;
4. Cardiovascular Research Center, Massachusetts General Hospital, Boston, MA, USA;
5. Centro Nacional de Investigaciones Cardiovasculares (CNIC), Madrid, Spain;
6. Center for Heart Lung Innovation, University of British Columbia, Vancouver;
7. Department of Medicine, Harvard Medical School, Boston, MA, USA;
8. Department of Surgery, Perelman School of Medicine, University of Pennsylvania, Philadelphia, PA, USA;
9. Center for Cardiometabolic Disease Prevention, Baylor College of Medicine, Houston, TX, USA;
10. Department of Medical Oncology, Dana-Farber Cancer Institute, Boston, MA, USA;
11. Department of Pathology, Brigham and Women's Hospital, Boston, MA, USA;
12. Department of Hematology, Brigham and Women's Hospital, Boston, MA, USA;
13. Icahn School of Medicine at Mount Sinai, New York, NY, USA;
14. Department of Biostatistics, Yale School of Public Health, New Haven, CT;
15. Division of Genetic Medicine, Department of Medicine, Vanderbilt University Medical Center, TN, USA;
16. CIBER en Enfermedades Cardiovasculares (CIBER-CV), Madrid, Spain;
17. Malcolm Randall VA Medical Center, Gainesville, FL;
18. Division of Vascular Surgery, University of Florida College of Medicine, FL, USA

* Co-first authors
§ Equally supervised this work

Corresponding Authors:
Jose J. Fuster, PhD
jjfuster@cnic.es
Melchor Fernández Almagro, 3
28029 - Madrid (Spain)
Tel: (+34) 914531200, ext 4304
Fax: (+34) 914531265
Twitter: @josejfuster
ORCID: 0000-0002-5970-629X

Derek Klarin, MD
derek.klarin@surgery.ufl.edu
1600 SW Archer Road, NG-45, PO Box 100128, Gainesville, FL 32610
Tel: 352-273-5485
Fax: 352-273-5515
ORCID: 0000-0002-4636-5780

Main Text Total word count: 3,517

Funding: P.N. is supported by a Hassenfeld Scholar Award from the Massachusetts General Hospital, grants from the National Heart, Lung, and Blood Institute (R01HL1427, R01HL148565, and R01HL148050), and from Fondation Leducq (TNE-18CVD04). S.M.Z is supported by the NIH National Heart, Lung, and Blood Institute (1F30HL149180-01) and the NIH Medical Scientist Training Program Training Grant (T32GM136651). A.G.B. is supported by a Burroughs Wellcome Fund Career Award for Medical Scientists, a NIH Director Early Independence Award (DP5-OD029586) and a NHLBI BioData Catalyst Fellowship (OT3 HL147154-01). J.P.P is supported by a John S LaDue Memorial Fellowship. K.P. is supported by NIH grant 5-T32HL007208-43. J.J.F. is supported by grants RYC-2016-20026 and RTI2018-093554-A-I00) from the Spanish "Ministerio de Ciencia e Innovación", a 2019 Leonardo Grant for Researchers and Cultural Creators from the BBVA Foundation, the European Research Area Network on Cardiovascular Diseases CHEMICAL (grant AC19/00133 from the "Spanish Instituto de Salud Carlos III") and the Leducq Foundation (TNE-18CVD04). The project leading to these results received funding from "la Caixa" Foundation (ID 100010434), under agreement HR17-00267. The Centro Nacional de Investigaciones Cardiovasculares (CNIC) is supported by the Instituto de Salud Carlos III (ISCIII), the Ministerio de Ciencia e Innovación and the Pro CNIC Foundation. P.L. receives funding support from the National Heart, Lung, and Blood Institute (1R01HL134892), the American Heart Association (18CSA34080399), the RRM Charitable Fund, and the Simard Fund.

Disclosures: P.N. reported grants from Amgen during the conduct of the study and grants from Boston Scientific; grants and personal fees from Apple; personal fees from Novartis and Blackstone Life Sciences; and spousal employment at Vertex all outside the submitted work. P.L. is an unpaid consultant to, or involved in clinical trials for Amgen, AstraZeneca, Baim Institute, Beren Therapeutics, Esperion, Therapeutics, Genentech, Kancera, Kowa Pharmaceuticals, Medimmune, Merck, Norvo Nordisk, Merck, Novartis, Pfizer, Sanofi-Regeneron. Dr. Libby is a member of scientific advisory board for Amgen, Corvidia Therapeutics, DalCor Pharmaceuticals, Kowa Pharmaceuticals, Olatec Therapeutics, Medimmune, Novartis, and XBiotech, Inc. P.L.'s laboratory has received research funding in the last 2 years from Novartis, he is on the Board of Directors of XBiotech, Inc, and has a financial interest in Xbiotech, a company developing therapeutic human antibodies. These interests were reviewed and are managed by Brigham and Women's Hospital and Partners HealthCare in accordance with their conflict of interest policies. The other authors do not report any disclosures.

Acknowledgments: Thanks to the participants and staff of the UK Biobank and Mass General Brigham Biobank. UK Biobank analyses were conducted using Application 7089. Thanks to Dr. Zeyan Liew and teaching fellow Jiajun Lu, the instructors of the causal inference course at Yale.

Abbreviations: CHIP, clonal hematopoiesis of indeterminate potential; PAD, peripheral artery disease

92 **Abstract**

93 **Background**: Somatic mutations in blood indicative of clonal hematopoiesis of indeterminate
94 potential (CHIP), particularly in *DNMT3A*, *TET2*, and *JAK2*, are associated with an increased
95 risk of hematologic malignancy, coronary artery disease, and all-cause mortality. However,
96 whether CHIP is associated with increased risk of peripheral artery disease (PAD) remains
97 unknown. In addition, chemotherapy frequently causes mutations in DNA Damage Repair
98 (DDR) genes *TP53* and *PPM1D*, and whether CHIP caused by somatic mutations in DDR genes
99 results in increased risk of atherosclerosis is unclear. We sought to test whether CHIP, and CHIP
100 caused by DDR genes, associates with incident peripheral artery disease (PAD) and
101 atherosclerosis.

102 **Methods:** We identified CHIP among 50,122 exome sequences in individuals from UK and
103 Mass General Brigham Biobanks and tested CHIP status (N=2,851) with incident PAD and
104 atherosclerosis across multiple arterial beds. To mimic the human scenario of clonal
105 hematopoiesis and test whether the expansion of p53-deficient hematopoietic cells contributes to
106 atherosclerosis, a competitive bone marrow transplantation (BMT) strategy was used to generate
107 atherosclerosis-prone *Ldlr*-/- chimeric mice carrying 20% *Trp53*-/- hematopoietic cells (20%
108 KO-BMT mice). We then evaluated aortic plaque burden and plaque macrophage accumulation
109 12 weeks after grafting.

110 **Results:** CHIP associated with incident PAD (HR 1.7; $P=2.2x10^{-5}$) and atherosclerosis in
111 multiple beds (HR 1.3; $P=9.7x10^{-5}$), with increased risk among individuals with DDR CHIP (HR
112 2.0; P=0.0084). Among atherosclerosis-prone *Ldlr* null mice, the p53 -/- 20% KO-BMT mice
113 demonstrated increased aortic plaque size (p=0.013) and accumulation of p53-/- plaque
114 macrophages (P<0.001), driven by an abundance of p53-deficient plaque macrophages. The

expansion of p53-deficient cells did not affect the expression of the pro-inflammatory cytokines IL-6 and IL-1β in the atherosclerotic aortic wall.

Conclusions: Our findings highlight the role of CHIP as a broad driver of atherosclerosis across the entire arterial system, with evidence of increased plaque among p53 -/- 20% KO-BMT mice via expansion of plaque macrophages. These observations provide new insight into the link between CHIP and cardiovascular disease, and lend human genetic support to the concept that post-cytotoxic chemotherapy patients may benefit from surveillance for atherosclerotic conditions in addition to therapy-related myeloid neoplasms.

Abstract Word Count: 346

Key Words: somatic, atherosclerosis, clonal hematopoiesis, sequencing

139 **Introduction**

140 Peripheral artery disease (PAD) is a leading cause of cardiovascular morbidity and mortality
141 worldwide, and age is among its strongest risk factors. PAD associates with an extremely high
142 cardiovascular mortality and unmitigated can progress to limb loss[1]. The age-related acquisition
143 and expansion of leukemogenic mutations in hematopoietic stem cells has recently been
144 associated with an increased risk of hematologic malignancy, coronary artery disease, and
145 overall mortality[2, 3]. This phenomenon, termed clonal hematopoiesis of indeterminate potential
146 (CHIP), is relatively common in asymptomatic older adults, affecting at least 10% of individuals
147 older than 70 years of age[4]. CHIP mutations most frequently occur in epigenetic regulators
148 *DNMT3A* and *TET2,* in DNA damage repair (DDR) genes *PPM1D* and *TP53*, or cell cycle and
149 transcriptional regulator genes *JAK2* and *ASXL1*[5]. CHIP associates with coronary artery disease
150 in multiple studies[2, 6]. Whether CHIP links with increased risk of atherosclerosis in the peripheral
151 arterial bed (PAD) is unknown.

152 Here, we leveraged 50,122 whole exome sequences from two genetic biobanks (UK
153 Biobank [UKB], Mass General Brigham Biobank [MGBB]) and tested whether CHIP was
154 associated with increased risk of PAD and atherosclerosis across multiple arterial beds, and
155 additionally whether these associations varied by putative CHIP driver gene. Based on these
156 results, we then performed functional analyses in *Ldlr*-null mice transplanted with 20% *Trp53*-/-
157 bone marrow cells, a murine model of atherosclerosis and clonal hematopoiesis driven by *TP53*
158 mutations.

159

160 **Methods**

161 *Cohorts and exclusion criteria*

162 The UKB is a population-based cohort of approximately 500,000 participants recruited from
163 2006-2010 with existing genomic and longitudinal phenotypic data and median 10-year follow-
164 up[7]. Baseline assessments were conducted at 22 assessment centres across the UK with sample
165 collections including blood-derived DNA. Of ~49,960 individuals with WES data available, we
166 analyzed 37,657 participants consenting to genetic analyses after our exclusion criteria. Use of
167 the data was approved by the Massachusetts General Hospital Institutional Review Board
168 (protocol 2013P001840) and facilitated through UK Biobank Application 7089.
169 The MGBB contains genotypic and clinical data from >105,000 patients who consented
170 to broad-based research across 7 regional hospitals and median 3-year follow-up[8]. Baseline
171 phenotypes were ascertained from the electronic medical record and surveys. We analyzed
172 12,465 individuals consenting to genetic analysis after our exclusion criteria. Use of the data was
173 approved by the Massachusetts General Hospital Institutional Review Board (protocol
174 2020P000904).
175 Across both cohorts, we excluded individuals with prevalent hematologic cancer,
176 individuals without genotypic-phenotypic sex concordance, and one of each pair of 1st or 2nd
177 degree relatives at random. For the UKB, samples were further restricted to individuals with
178 Townsend deprivation index, a marker of socioeconomic status, available for analysis. Follow-up
179 time was defined as time from enrollment to disease diagnosis for cases, or to censorship or
180 death for controls.
181
182 *Whole exome sequencing and CHIP calling*
183 UKB WES were generated from whole blood-derived DNA at the Regeneron Sequencing
184 Center[9]. MGBB WES were generated using whole blood-derived DNA using Illumina

185 sequencing (mean coverage 55x). Somatic CHIP variants were detected with GATK MuTect2
186 software with parameters as previously described[6, 10]. Common germline variants and sequencing
187 artifacts were excluded as before. Samples were annotated with the presence of any CHIP if
188 MuTect2 identified one or more of a pre-specified list of pathogenic somatic variants, as
189 previously described[11, 12]. Additionally, samples were annotated with the presence of Large
190 CHIP (variant allele frequency >10%), as larger CHIP clones have previously been more
191 strongly associated with adverse clinical outcomes[6].
192
193 *Phenotype definitions*
194 Across both UKB and MGBB, PAD was defined by grouping together ICD-10 and ICD-9 billing
195 codes for aortic atherosclerosis (I70), peripheral vascular disease (I73.8, I73.9), and operative
196 procedures including amputation of leg (X09.3-5), bypass of artery of leg (L21.6, L51.3, L51.6,
197 L51.8, L59.1-8), endarterectomy or angioplasty of leg artery (L52.1-2, L54.1,4,8, L60.1-2,
198 L63.1,5), and other transluminal operations on leg arteries or peripheral stent placement
199 (L63.9,L66.7), as previously described[13]. Additionally, in the UKB self-reported peripheral
200 vascular disease, leg claudication/intermittent claudication, arterial embolism, femoral-popliteal
201 leg artery bypass, leg artery angioplasty +/- stent, or amputation of leg were also incorporated
202 (Data fields 20002, 20004) as performed previously[13]. Coronary artery disease and cerebral
203 atherosclerosis phenotype definitions for each cohort are detailed in **Tables I and II in the**
204 **supplement**. Other atherosclerotic conditions were defined using the Phecode Map 1.2[14] ICD-9
205 (https://phewascatalog.org/phecodes) and ICD-10 (https://phewascatalog.org/phecodes_icd10)
206 phenotype groupings for "abdominal aortic aneurysm", "aortic aneurysm", "other aneurysm",
207 "chronic vascular insufficiency of intestine", "acute vascular insufficiency of intestine",

208 “atherosclerosis of renal artery”. The composite atherosclerosis phenotype was created by
209 combining all analyzed atherosclerosis phenotypes (including PAD, coronary artery disease,
210 cerebral atherosclerosis, abdominal aortic aneurysm, aortic aneurysm, other aneurysm, chronic
211 vascular insufficiency of intestine, acute vascular insufficiency of intestine, and atherosclerosis
212 of renal artery) into one phenotype, whereby the first instance across all of these phenotypes was
213 used to determine time of first diagnosed atherosclerotic disease for survival analysis. Other
214 phenotypic covariates (never/prior/current smoking status, hypertension, hyperlipidemia,
215 principal components of ancestry, etc.) were used as previously defined[15].
216
217 *Association Analysis*
218 In the UKB and MGBB a traditional cox-proportional hazards model was utilized using the
219 Survival package in R-3.5 adjusting for age, age^2, sex, smoking status, normalized Townsend
220 deprivation index as a marker of socioeconomic status (only available in UKB), and the first ten
221 principal components of genetic ancestry. Demographic and clinical characteristics found to
222 differ between individuals with and without CHIP were tested using chi-squared (categorical)
223 and Wilcoxon-rank sum (continuous) tests with a two-tailed $P< 0.05$ determining significance.
224 Sensitivity analysis including other covariates (normalized BMI, prevalent hypertension,
225 prevalent Type 2 diabetes, and prevalent hyperlipidemia) was not found to significantly change
226 associations with PAD in the UKB (**Figure I in the supplement**). Additional sensitivity
227 analyses were utilized in the UKB including propensity score adjustment, as well as a marginal
228 structural cox proportional hazards model estimated through stabilized inverse-probability-
229 treatment-weight (IPTW)[16] to estimate the total causal effect of CHIP on PAD. Further details of
230 propensity score methods and stabilized IPTW analysis are described in the supplementary

231 appendix. For our primary outcome PAD, results were combined across the UKB and MGBB
232 using an inverse-variance weighted fixed effects meta-analysis, a two tailed association $P < 0.05$
233 determined statistical significance. In our secondary analysis of CHIP with 10 additional,
234 incident atherosclerotic diseases, a two-tailed Bonferroni p-value threshold of $P<0.05/10=0.005$
235 was used to declare statistical significance.
236
237 *Mice*
238 Animal experiments followed protocols approved by the Institutional Ethics Committee
239 at the Centro Nacional de Investigaciones Cardiovasculares and conformed to EU Directive
240 86/609/EEC and Recommendation 2007/526/EC regarding the protection of animals used for
241 experimental and other scientific purposes, enforced in Spanish law under Real Decreto
242 1201/2005. All mice were maintained on a 12-h light/dark schedule in a specific pathogen-free
243 animal facility in individually ventilated cages and given food and water ad libitum. C57Bl/6J
244 *Trp53*-/- mice were obtained from the Jackson Laboratory. *Ldlr*-/- mice carrying the CD45.1
245 isoform of the CD45 hematopoietic antigen were generated by crossing LDLR-KO mice from
246 the Jackson Laboratory and B6.SJL-*PtprcaPepcb*/BoyCrl mice from Charles River Laboratories.
247 *Competitive bone marrow transplantation and atherosclerosis induction in mice*
248 CD45.1+ *Ldlr*-/- recipients were transplanted with suspensions of BM cells containing 20%
249 CD45.2+ *Trp53*-/- cells and 80% CD45.1+ *Trp53*+/+ cells (20% KO-BMT mice) or 20 %
250 CD45.2+ *Trp53*+/+ cells and 80% CD45.1+ *Trp53*+/+ cells (20% WT-BMT mice) similar to
251 previous studies[17] (**Figure II in the supplement**). BM cells were isolated from femurs and tibias
252 of donor mice after euthanasia. Recipient *Ldlr*-/- mice were exposed to two doses of 450 rad
253 three hours apart. After the second irradiation, each recipient mouse was injected

254 with 10^7 BM cells i.v. Water was supplemented with antibiotics for 7 days before transplant and
255 for 14 days post-transplant. Mice that did not recover full pre-irradiation body weight 28 days
256 after transplant were excluded from further analysis. Starting four weeks after BMT, mice were
257 fed a high fat high cholesterol (HF/HC) Western diet (Harlan-Teklad, TD.88137, Adjusted
258 Calories Diet; 42% from fat, 0.2% cholesterol) to promote hypercholesterolemia and the
259 development of atherosclerosis. Mice were maintained on a HF/HC diet for 9 weeks
260
261 *Quantification of aortic atherosclerosis burden in mice*
262 Mice were euthanized and aortas were removed after in situ perfusion with phosphate-buffered
263 saline injected through the left ventricle of the heart. Tissue fixation was achieved by immersion
264 in 4% paraformaldehyde in PBS overnight at 4°C. Aortic tissue was then dehydrated and
265 embedded in paraffin for sectioning. Histological sections comprising the aortic root as
266 determined by the location of the aortic valve leaflets were cut at a thickness of 4 μm or 6 μm.
267 An operator who was blinded to genotype quantified plaque size in aortic root sections by
268 computer-assisted morphometric analysis of microscopy images. For each mouse, atherosclerotic
269 plaque size in aortic root cross-sections was calculated as the average of 5 independent sections
270 separated by ∼16μm. Atherosclerotic plaque composition was examined by
271 immunohistochemical techniques. Vascular smooth muscle cells were identified with an alkaline
272 phosphatase-conjugated mouse anti-smooth muscle α-actin (SMA) monoclonal antibody (clone
273 1A4, SIGMA) and Vector Red Alkaline Phosphatase Substrate (Vector Laboratories).
274 Macrophages were detected with a rabbit anti-Mac2 monoclonal antibody (Santa Cruz
275 Biotechnologies), a biotin-conjugated goat anti-rat secondary antibody and streptavidin-HRP,
276 DAB substrate (all from Vector Laboratories), with hematoxylin counterstaining. Collagen

277 content was determined by a modified Masson's trichrome staining. Microscopy images were
278 analyzed using ImageJ software using the Color Deconvolution plugin. Plasma was collected in
279 EDTA-coated tubes and cholesterol levels were determined using an enzymatic assay
280 (Cholesterol E, WAKO Diagnostics).
281
282 *Flow cytometry analyses of blood and tissue samples.*
283 Peripheral blood was obtained from the facial vein and collected into EDTA-coated tubes. Bone
284 marrow cells were flushed out of two femurs and two tibias per mouse. Aortic arches were
285 digested for 45 minutes at 37°C in RPMI containing 10% FBS and 0.25 mg/ml Liberase TM
286 (Roche Life Science). Red blood cells were lysed in all samples by treatment with 1X Red Blood
287 Cell Lysis Buffer (eBioscience ThermoFisher) for 5 minutes on ice. Bone Marrow lineage-
288 negative cells were defined as negative for CD11b, Gr-1, Ter119, B220, CD3e and CD127. Bone
289 marrow HSPCs were defined as Lineage-, c-Kit+, Sca1+. Blood classical monocytes were
290 identified as CD45+, CD115^{Hi}, CD43^{Lo}, Ly6c^{Hi}; patrolling monocytes, as CD45+, CD115^{Hi},
291 CD43^{Hi}, Ly6c^{Lo}; neutrophils, as CD45+, CD115^{Int}, Ly6g+; T lymphocytes, as CD45+, CD115-,
292 B220-, CD3+; B lymphocytes, as CD45+, CD115-, CD3-, B220+; and aortic macrophages, as
293 CD45+, CD3-, Ly6g-, CD11B+, F4/80Hi. Gating strategies can be found in our previous
294 publications[17, 18]. Samples were stained with combinations of biotinylated and/or fluorescently
295 labeled antibodies in PBS with 1% FBS for 30 min on ice. The following fluorescent antibodies
296 were used for staining and flow cytometry analysis: eFluor450-conjugated anti-CD45.2, FITC-
297 conjugated anti-CD45.2, Pe-Cy7-conjugated anti-CD45.1, FITC-conjugated anti-CD11b,
298 eFluor450-conjugated anti-CD11B, PE-conjugated anti-CD115, PE-eFluor610-conjugated anti-
299 CD3, FITC-conjugated anti-CD4 (from eBioscience); APC-Cy7-conjugated anti- B220, PerCP-

300 Cy5.5-conjugated anti-Ly6G, BV510-conjugated anti-Ly6G, BV711-conjugated anti-CD43, PE-
301 Cy7-conjugated anti-c-Kit, AlexaFluor647-conjugated anti-Sca-1 (from BD Biosciences); PE-
302 conjugated anti-F4/80 (from R&D Systems); PerCP-Cy5.5-conjugated anti-CD45.1, BV510-
303 conjugated anti-CD8a, PerCP-Cy5.5-conjugated anti-mouse Ki-67 (from BioLegend).
304 Fixation/permeabilization for Ki-67 intracellular staining was achieved using commercially
305 available kits following manufacturer's instructions (Foxp3 Transcription Factor Staining Buffer
306 Set, eBioscience ThermoFisher). Dead cells were excluded from analysis by DAPI staining in
307 unfixed samples and by LIVE/DEAD Fixable Near-IR staining (ThermoFisher Scientific) in
308 fixed samples. BD LSRFortessa and BD FACSymphony Cytometers (BD Bioscience) were used
309 for data acquisition. Data were analyzed with FlowJo Software.
310
311 *Murine macrophage culture and cell cycle analysis*
312 Bone marrow-derived macrophages (BMDM) were obtained from suspensions of femoral BM
313 and differentiated for 7 days in the presence of RPMI Medium supplemented with antibiotics,
314 10% fetal bovine serum and 100 ng/ml MCSF. For cell-cycle analysis, MCSF concentration in
315 cell culture medium was decreased to 5 ng/ml for 48h to induce progressive synchronization of
316 macrophages in G0 phase (i.e. quiescence) and cell cycle re-entry was induced by treatment with
317 100 ng/ml MCSF. Macrophages were trypsinized and collected by centrifugation for 5 minutes at
318 300g. After fixation in 80% ethanol for 1 h at -20ºC, cells were incubated for at least 30 minutes
319 with 50 µg/mL propidium iodide containing 0.25 mg/mL RNAse A (both from SIGMA).
320 Labelled cells were analyzed in a BD LSRFortessa flow cytometer BD Bioscience and DNA
321 histograms were fitted into cell cycle distributions using ModFit 3.0 software (Verity Software
322 House).

323
324 *Gene expression analysis by quantitative real-time PCR (qPCR) and Western Blot.*
325
326 Total RNA from aortic arch tissue was isolated using Trizol reagent and RNeasy kits (QIAGEN).
327 RNA (1 μg) was reverse transcribed with High-Capacity cDNA Reverse Transcription Kit
328 (Applied Biosystems) and qPCR was performed with SYBR® Green PCR Master Mix (Applied
329 Biosystems) in a AB7900 Real time PCR system. Results were analyzed with the ΔΔCt method.
330 The average of 36B4 and β-actin was used as reference for normalization. Primer sequences can
331 be found in our previous publication[17]. For Western Blot analysis of protein levels, protein
332 extracts from cultured macrophages were obtained using ice-cold lysis buffer (20mM Tris-HCl
333 pH 7.5, 150 mM NaC, 1 mM NA2EDTA, 1 mM EGTA, 1% Triton) supplemented with protease
334 and phosphatase inhibitors (Roche Applied Science). Equal amounts of protein lysates were
335 resolved by SDS-PAGE and the following antibodies were used for immunoblotting: anti-p53
336 (Cell Signaling, #32532S, dil 1/1000) and HRP anti-alpha tubulin (AbCam, #ab40742, dil
337 1/2000). An ImageQuant LAS 4000 biomolecular imaging system (GE Healthcare) was used for
338 image acquisition and the ImageJ software was used for band densitometric analysis.
339
340 *Statistical analysis of data in experimental studies*
341 Data are shown as mean ± SEM unless otherwise stated. Statistical significance of differences in
342 experiments with two groups and only one variable was assessed by unpaired Student's t tests
343 (with Welch correction for unequal variance when appropriate) or Mann-Whitney U Tests.
344 Differences in experiments with more than one independent variable were evaluated by two-way
345 analysis of variance (ANOVA) with post-hoc Sidak's multiple comparison tests. All statistical
346 tests were performed using GraphPad Prism software (GraphPad Software Inc.).
347

348 **Results**

349 *Study Cohorts and Risk Of Hematologic Malignancy*

350 After excluding individuals with a known history of hematologic malignancy at enrollment, we
351 identified 37,657 unrelated individuals from the UKB and 12,465 individuals from MGBB with
352 whole exome sequencing data available for downstream analysis. Using a previously validated
353 somatic variant detection algorithm[10], we identified 2,194 (5.8%) and 657 (5.4%) CHIP carriers
354 in the UKB and MGBB, respectively (**Table III in the supplement**). Demographic and clinical
355 characteristics of these individuals, stratified by CHIP status, are depicted in **Table IV in the**
356 **supplement**. CHIP carriers tended to be older, male, previous smokers, and have a history of
357 coronary artery disease, hypertension, and hyperlipidemia (two-tailed chi-squared and Wilcoxon-
358 rank sum $P< 0.05$).

359 We first replicated known CHIP associations[10] with white blood cell (Beta 0.09 SD; 95%
360 CI 0.05-0.13; $P=1.6x10^{-5}$), monocyte (Beta 0.05 SD; 95% CI 0.01-0.09; P=0.009), neutrophil
361 (Beta 0.10 SD; 95% CI 0.06-0.14; $P=2.1x10^{-6}$), and platelet counts (Beta 0.07 SD; 95% CI 0.03-
362 0.11; P=0.0005) in UKB, with larger CHIP clone size as measured by variant allele fraction
363 (VAF) having stronger effects on blood counts (**Figure III in the supplement**). Consistent with
364 the existing literature[5, 10], CHIP also associated with incident hematologic malignancy (HR 2.20;
365 95% CI 1.70-2.85; $P=1.8x10^{-9}$) - specifically for acute myeloid leukemia (HR 8.08; 95% CI
366 4.36-14.97; $P=3.2x10^{-11}$), myeloproliferative neoplasms (HR 5.89; 95% CI 3.69-9.89; $P=9.7x10^{-}$
367 ^{14}), and polycythemia vera (HR 12.37; 95% CI 4.85-31.54; $P=1.4x10^{-7}$). This risk increased with
368 larger VAF (**Figure IV in the Supplement**).

369

370 *CHIP and Incident PAD Risk*

371 We next tested the association of CHIP status with incident PAD. Using available electronic
372 health record (EHR) data and a previously validated PAD definition[13], we identified 338 and 419
373 incident PAD cases in UKB and MGBB, respectively. CHIP associated with a 58% increased
374 risk of incident PAD in the UKB (HR_{UKB} = 1.58, 95% CI: 1.11-2.25; P=0.01, **Figure 1**), results
375 that were replicated in MGBB (Overall HR = 1.66, 95% CI: 1.31-2.11; $P=2.4x10^{-5}$). We then
376 sought to evaluate whether those with larger CHIP clone sizes (i.e., higher VAF) had greater risk
377 for PAD, as larger CHIP clones associate more strongly with adverse clinical outcomes[6]. We
378 observed a graded relationship between CHIP VAF and PAD, as those with a VAF > 10% had
379 even greater risk for an incident PAD event (Overall HR = 1.97, 95% CI: 1.44-2.71; $P=2.3x10^{-5}$,
380 **Figure 1**). Additional sensitivity analyses, including propensity score adjustment and a marginal
381 structural Cox proportional hazards model estimated through stabilized inverse-probability-
382 treatment-weight revealed similar results in the UKB (**Figure V in the supplement**). Subsequent
383 analyses showed no significant interaction between CHIP status and either age, sex, or smoking
384 status on incident PAD risk.
385
386 *CHIP and Incident Atherosclerosis Across Multiple Vascular Beds*
387 We next assessed whether CHIP was associated with 9 other incident atherosclerotic
388 diseases across multiple vascular beds. Using EHR-based disease definitions[19], we tested the
389 association of CHIP with atherosclerotic disease across the mesenteric (acute and chronic),
390 coronary, and cerebral vascular beds, as well as with aneurysmal disease (aortic and any other
391 aneurysm). We observed significant associations for coronary artery disease (HR 1.40, 95% CI:
392 1.20 to 1.63; $P=1.9x10^{-5}$), any aortic aneurysm (HR 1.74; 95% CI: 1.21 to 2.51; P=0.0028), other
393 aneurysms (HR 1.70; 95% CI: 1.23 to 2.34; P=0.0013), and chronic mesenteric ischemia (HR

394 9.12; 95% CI: 2.34 to 35.63; P=0.0015) across both cohorts, with directionally consistent effect
395 estimates observed for all the tested phenotypes (**Figure 2a**). These associations were
396 consistently stronger for large CHIP clones (**Figure VI in the supplement)**. We then created a
397 composite, incident atherosclerosis outcome combining all nine atherosclerotic phenotypes
398 ("pan-arterial atherosclerosis", **Table V in the Supplement**). CHIP associated with this
399 combined incident pan-arterial atherosclerosis endpoint (HR 1.31, 95% CI: 1.14 to 1.49,
400 $P=9.7x10^{-5}$), again with stronger effects conferred by large CHIP clones (HR 1.45; 95% CI: 1.20
401 to 1.75; P=0.00013) (**Figure 2b,c**).
402
403 *Gene-specific analyses of CHIP with incident atherosclerotic diseases*
404 Next, we sought to understand whether the clonal hematopoiesis putative driver gene
405 differentially affected the risk of acquiring atherosclerosis. Previous work has focused primarily
406 on the epigenetic regulators *DNMT3A* and *TET2*[3, 17], and whether DDR CHIP confers an
407 increased risk of atherosclerosis is unknown. We stratified the CHIP-PAD and CHIP pan-arterial
408 atherosclerosis analyses by putative driver genes and specific mutations - focusing on *DNMT3A*,
409 *TET2*, *ASXL1*, *JAK2*, the DDR genes *PPM1D* and *TP53*, and mutations that specifically disrupt
410 splicing factor genes *(LUC7L2, PRPF8, SF3B1, SRSF2, U2AF1,* and *ZRSR2)*[20]. We observed an
411 association of CHIP with PAD across the four common CHIP genes (*DNMT3A*, *TET2*, *ASXL1*,
412 and *JAK2*), with significant heterogeneity of incident PAD effect sizes across the CHIP genes
413 ($P_{heterogeneity} = 0.03$) (**Figure 3a**). This heterogeneity persisted in sensitivity analysis after
414 excluding *JAK2* carriers ($P_{heterogeneity} = 0.046$). These data also revealed the novel finding that
415 DDR *TP53* and *PPM1D* CHIP associates with incident PAD (HR 2.72; 95% CI: 1.20 to 1.75;
416 P=0.00013) and incident CAD (HR 2.51; 95% CI: 1.52-4.14; P=0.00032), with a stronger effect

417 on PAD conferred by *TP53* (HR 4.98; 95% CI: 1.23-20.09; P=0.024, **Figure 3a-c).** Similar
418 findings were observed for the incident pan-arterial atherosclerosis outcome when stratifying by
419 putative driver gene (**Figure VII in the supplement**). Further sensitivity analysis for DDR-
420 CHIP and incident PAD when excluding solid organ malignancy did not significantly change the
421 associations ($P_{heterogeneity} > 0.05$).
422
423 *Atherosclerosis development in p53-/ CHIP mice*
424 Based on our gene specific findings, we next further characterized the effects of reduced function
425 of hematopoietic p53 in atherosclerotic mice. To mimic CHIP and test whether the expansion of
426 p53-deficient hematopoietic cells contributes to atherosclerosis, a competitive bone marrow
427 transplantation (BMT) strategy was used to generate atherosclerosis-prone *Ldlr*-/- chimeric mice
428 carrying 20% *Trp53*-/- hematopoietic cells (20% KO-BMT mice). These mice then consumed a
429 high fat/high cholesterol diet for 9 weeks to induce atherosclerosis development. To distinguish
430 donor *Trp53*-/- and *Trp53*+/+ cells in this experimental setting, *Trp53*+/+ cells were obtained
431 from mice carrying the CD45.1 variant of the CD45 hematopoietic antigen, whereas *Trp53*-/-
432 cells were obtained from mice carrying the CD45.2 variant of this protein. Control mice (20%
433 WT-BMT) were transplanted with 20% CD45.2+ *Trp53*+/+ cells and 80% CD45.1+ *Trp53*+/+
434 cells (**Figure 4a and Figure II in the supplement**). Flow cytometry analysis of CD45.2+ blood
435 cells established that this BMT strategy led to a modest, but significant expansion of donor
436 *Trp53*-/- BM-derived cells compared to *Trp53*+/+ cells in both BM hematopoietic
437 stem/progenitor cells (HSPCs) and circulating white blood cells (**Figure 4B,C**), consistent with
438 previous studies[21-23]. Transplanted *Trp53*-/- BM cells expanded into all blood cell lineages to a
439 similar extent, but this relative expansion did not affect absolute blood cell counts (**Figure VIII**

440 **in the supplement**). Having validated this mouse model of p53 CHIP based on a competitive
441 BMT strategy, we next assessed whether this phenomenon affects the development of
442 atherosclerosis or related metabolic abnormalities. The presence and expansion of *Trp53*-/- cells
443 led to a significant ~40% increase in plaque size in the aortic root of male *Ldlr*-/- mice (**Figure**
444 **4D**), without affecting body weight, spleen weight or serum cholesterol levels (**Figure VIII in**
445 **the supplement, C-E**). Similar results were obtained in female *Ldlr*-/- mice (**Figure IX in the**
446 **supplement**). In contrast to previous work on *DNMT3A/TET2* CHIP, the expansion of p53-
447 deficient cells[12, 17, 18, 24, 25] did not affect the expression of the pro-inflammatory cytokines IL-6
448 and IL-1β in the atherosclerotic aortic wall (**Figure X in the supplement**).
449
450 *Proliferation and expansion of p53-deficient macrophages in the murine atherosclerotic aorta*
451 Increased atherogenesis in mice carrying *Trp53*-/- cells was paralleled by a substantial increase
452 in plaque macrophage content, as assessed by immunohistological staining of Mac2, with no
453 significant changes in other cell components (**Figure 5A**), suggesting a contribution of increased
454 arterial macrophage burden to accelerated atherosclerosis in conditions of p53 CHIP. Flow
455 cytometry analysis of matched samples from blood and digested atherosclerotic aortae from
456 20% KO-BMT mice revealed substantially higher chimerism in aortic macrophages (~76%
457 *Trp53*-/-) than in blood classical monocytes (~48%), the major source of plaque macrophages
458 (**Figure 5B**). This expansion of p53-deficient macrophages within the vascular wall was
459 paralleled by a 2-fold increase in the frequency of proliferating cells within the CD45.2+ *Trp53*-
460 /- aortic macrophage population compared to CD45.2+ *Trp53*+/+ macrophages, as assessed by
461 flow cytometry analysis of the proliferation-related antigen Ki-67 (**Figure 5C).** Consistent with
462 our observations *in vivo*, cultured *Trp53*-/- macrophages exhibit accelerated mitotic cell cycle

463 progression, with a >2-fold increase in the percentage of S-phase cells upon stimulation with
464 macrophage colony stimulating factor (MCSF), a major determinant of plaque macrophage
465 proliferation[26] (**Figure 5D**). *Trp53* expression analysis suggests a central role of p53 in the
466 normal regulation of macrophage cell cycle progression, as p53 was expressed in quiescent
467 macrophages at the transcript and protein level and further induced after MCSF stimulation
468 (**Figure 5E,F**). Furthermore, p53-deficient macrophages exhibited major changes in the
469 expression of pivotal regulators of cell cycle entry and progression, such as *Cdkn1a*/p21^{Cip1} and
470 Cyclin B1 (**Figure 5G**).
471

472 **Discussion**

473 This study combined exome sequencing data across two biobanks to detect somatic
474 mutations in over 50,000 individuals and observed that the presence of CHIP was significantly
475 associated with an increased risk of developing PAD and atherosclerosis across multiple arterial
476 beds. Increased risk was differentially observed across CHIP driver genes with evidence of a
477 graded relationship with CHIP VAF, with large CHIP clones conferring greater risk of disease.
478 Lastly, analysis of p53 CHIP using a BMT murine model showed increased aortic atherosclerotic
479 plaque among p53 CHIP carriers accompanied by expansion of plaque macrophages, supporting
480 a direct contribution of p53-mutant hematopoietic cells to accelerated atherogenesis.

481 These findings permit several conclusions. First, in humans, CHIP appears to promote
482 atherosclerosis across the entire arterial system. Previous work linked CHIP with increased risk
483 of coronary artery disease and early-onset MI[2, 3]. We build on these findings by demonstrating
484 that CHIP is also associated with PAD, and a composite pan-arterial atherosclerosis outcome
485 reflective of an increased burden of atherosclerosis throughout the human arterial system. In

486 addition, we observed suggestive CHIP associations with aneurysmal degeneration of the aorta.
487 The genetic and epidemiologic risk factors underlying atherosclerotic occlusive disease and
488 AAA overlap considerably[27], and substantial evidence implicates inflammation and macrophage
489 infiltration in driving this aortic disease[28]. The observed link between CHIP and aneurysmal
490 disease warrants further investigation in future studies.

491 Second, DDR gene CHIP appears to confer an increased risk of atherosclerotic
492 cardiovascular disease. In previous work, Jaiswal et al demonstrated an increased risk of
493 coronary artery disease among individuals with CHIP through *DNMT3A, TET2, ASXL1,* and
494 *JAK2* somatic driver mutations[3]. DDR CHIP is often observed among individuals following
495 cytotoxic chemotherapy for the treatment of malignancy and has been linked to the development
496 of therapy-related myeloid neoplasms, but limited evidence is available to inform clinical
497 decision making regarding whether DDR CHIP carriers have increased risk of cardiovascular
498 disease. The current study demonstrates that CHIP related to DDR-genes (*TP53, PPM1D*)
499 confers an increased risk of developing atherosclerosis. These findings lend human genetic
500 support to the concept that post-cytotoxic chemotherapy patients may benefit from surveillance
501 for atherosclerotic conditions in addition to therapy-related myeloid neoplasms.

502 Third, CHIP related to *TP53* mutations appears to drive atherosclerosis risk via expansion
503 of p53-deficient macrophages in occlusive plaque lesions. Previous experimental studies
504 assessed the role of p53 in atherogenesis using mice engineered to exhibit gain or loss of
505 function of p53 in the whole body or in specific cell types, with a variety of results[29-35]. Here we
506 demonstrate that carrying a fraction of p53-deficient blood cells is sufficient to accelerate
507 atherosclerosis development, as these cells have a selective advantage to expand, both in HSPCs
508 within the BM and in macrophages within the arterial wall, leading to increased macrophage

509 burden in the atherosclerotic plaque. Mechanistically, p53-deficient macrophage expansion
510 seems related to increased proliferation, a major driver of macrophage burden in atherosclerotic
511 plaques[36]. Although p53 expression is typically induced by DNA damage or other kinds of
512 cellular stress, we found that it is expressed in resting conditions in cultured macrophages and
513 further induced by mitogenic stimulation, suggesting a physiological role in the regulation of
514 macrophage cell cycle progression. Accordingly, p53-deficient macrophages exhibited
515 accelerated cell cycle kinetics. Overall, these experimental findings provide support to the notion
516 that *TP53* CHIP mutations contribute directly to accelerated atherosclerosis and highlight major
517 differences in the mechanisms underlying accelerated atherosclerosis in CHIP driven by
518 mutations in *TP53* or epigenetic regulators. Previous murine studies on *Tet2* CHIP showed that
519 TET2-deficient cells expand in bone marrow and blood, but not in the atherosclerotic plaque. In
520 contrast, we found that p53 exhibits a double competitive advantage, expanding in both the BM
521 and arterial wall, which suggests that small *TP53*-mutant blood clones may be sufficient to
522 accelerate atherosclerosis development. Evaluating this possibility will require additional studies
523 using high sensitivity sequencing strategies. Furthermore, in contrast to previous reports related
524 to *DNMT3A/TET2* CHIP[12, 17, 18, 24, 25], we did not observe a significant effect of p53 deficiency on
525 the expression of the pro-inflammatory cytokines IL-1β and IL-6. These results are consistent
526 with previous human data showing that circulating levels of pro-inflammatory cytokines are
527 significantly increased in carriers of CHIP driven by mutations in these epigenetic regulators, but
528 not in carriers of mutations in *TP53* or *PPM1D*[10]. These mechanistic differences between *TP53*-
529 CHIP and *DNMT3A/TET2*-CHIP require consideration when designing preventive care strategies
530 targeting the effects of CHIP on atherosclerosis. Thus, while the pathogenic effects of TET2-
531 CHIP may be prevented by targeting IL-1β-driven inflammation[17], accelerated atherosclerosis

532 associated with *TP53* mutations may be better tackled by other strategies. Additional
533 experimental and clinical studies should evaluate these opportunities for personalized medicine
534 in the context of CHIP.

535 Lastly, a recent publication has generated a novel hypothesis regarding the relationship
536 between CHIP and atherosclerosis[37]. In their analysis, Heyde et al. suggest that CHIP may be a
537 symptom of the atherosclerosis trait complex (the interplay of chronic inflammation,
538 hyperlipidemia, and arterial plaque), rather than a causal risk factor, based on murine and human
539 observations that atherosclerosis may accelerate HSC proliferation and somatic evolution. While
540 their study engenders an intriguing hypothesis, there are several observations in the literature and
541 in our current study that we believe do not support this interpretation. Firstly, in the Heyde et al.
542 study, *Ldlr*-null mice irradiated and transplanted with bone marrow of *Tet2* -/- mice that were fed
543 an atherogenic diet demonstrated greater *Tet2* -/- neutrophil and monocyte expansion than
544 similar mice fed normal chow. However, in marked contrast, we previously showed that *Tet2*-/-
545 cells expand similarly when *Ldlr*-null mice are fed either a high cholesterol diet or normal
546 chow[17]. Furthermore, in our prior work, the expansion of *Tet2*-/- cells was completely unaffected
547 by treatment with a pharmacological NLRP3 inhibitor, even though this inhibitor led to a 2-fold
548 decrease in atherosclerotic plaque size[17]. Secondly, in our current analysis of the pan-arterial
549 atherosclerosis endpoint, CHIP was associated with incident atherosclerotic events among a pool
550 of individuals without any history of atherosclerosis at baseline - suggesting that CHIP precedes
551 clinically significant occlusive disease. Thirdly, Heyde et al. state that the uniform hazard ratios
552 observed for the CHIP-coronary artery disease association provide supportive evidence for the
553 notion that atherosclerotic disease precedes the development of clonal hematopoiesis. However,
554 in our study we identify significant heterogeneity of incident PAD effect sizes when stratifying

555 by CHIP genes, as well as a dose-response relationship between CHIP clone size (or VAF) and
556 incidence of atherosclerosis, suggesting that CHIP genes vary in their effect on incident PAD
557 risk, and that expanded CHIP variants have a stronger influence on future atherosclerotic risk.
558 Thus, given the 1) association with incident atherosclerotic disease, 2) dose-response relationship
559 with CHIP clone size and heterogeneity by CHIP gene, and 3) that *TP53*, *TET2*, and *JAK2*[38]
560 appear to drive atherosclerosis through disparate mechanisms, clonal hematopoiesis acting as a
561 causal risk factor appears to be a more parsimonious explanation to unify these findings.

562 Several limitations merit mention. First, our PAD and cardiovascular disease phenotypes
563 are based on EHR data and may result in misclassification of case status. Such misclassification
564 would likely reduce statistical power for discovery and on average bias results toward the null.
565 Second, selection bias from differential loss-of-follow up, volunteer bias, and missingness in
566 covariates may be present given the nature of the genetic biobanks used in this study. Third,
567 while we maximized the number of participants in our analysis of CHIP and additional
568 atherosclerotic diseases, it may still have been underpowered for certain phenotypes. Lastly, the
569 cohorts in these studies are largely of European ancestry; while prior reports have not observed
570 significant phenotypic differences in CHIP associations by ancestry[5, 12], further epidemiological
571 studies in ethnically diverse individuals are required to ensure that this is the case for PAD as
572 well.

573 In conclusion, CHIP is associated with incident atherosclerosis in multiple vascular beds,
574 with murine evidence of increased plaque among *TP53* CHIP carriers through an expansion of
575 plaque macrophages (**Figure 6**). The observations presented here expand insight into CHIP-
576 mediated atherosclerosis. The novel finding that DDR gene CHIP plays a particular role in PAD
577 raises new questions regarding the mechanisms of regional heterogeneity of atherosclerotic

578 involvement in face of systemic exposure to traditional risk factors such as dyslipidemia,

579 hypertension, and smoking.

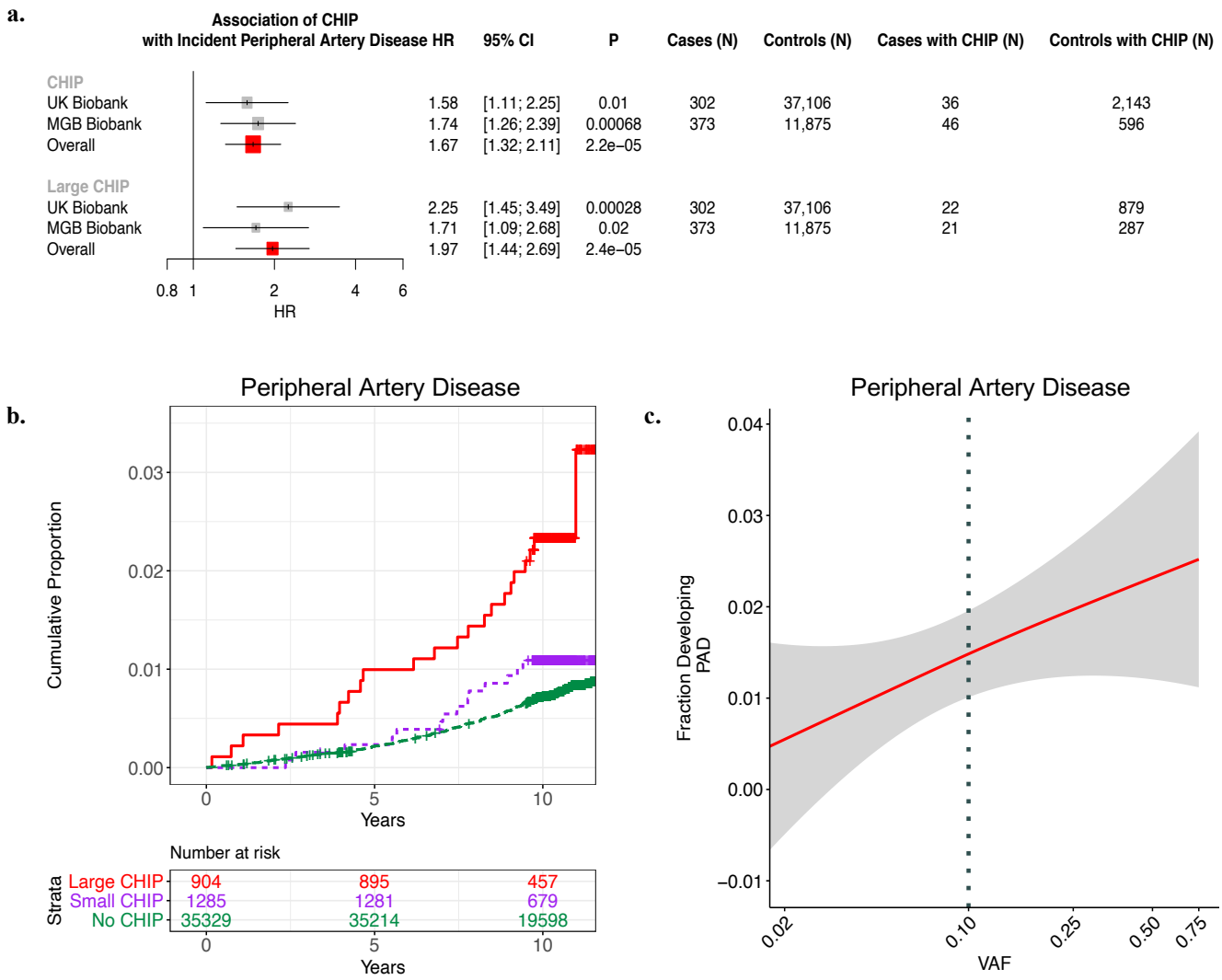

Figure 1. CHIP and incident PAD risk. a) Association of CHIP and large CHIP (VAF>10%) carrier state with incident PAD events in the UK Biobank (UKB) and Mass General Brigham Biobank (MGBB). Results were combined using an inverse-variance weighted fixed effects meta-analysis. b) Cumulative proportion of individuals developing PAD stratified by CHIP VAF clone size category in the UK Biobank. c) Fraction of individuals developing incident PAD by CHIP VAF in the UK Biobank. CHIP = clonal hematopoiesis of indeterminate potential; VAF = variant allele fraction; PAD = peripheral artery disease

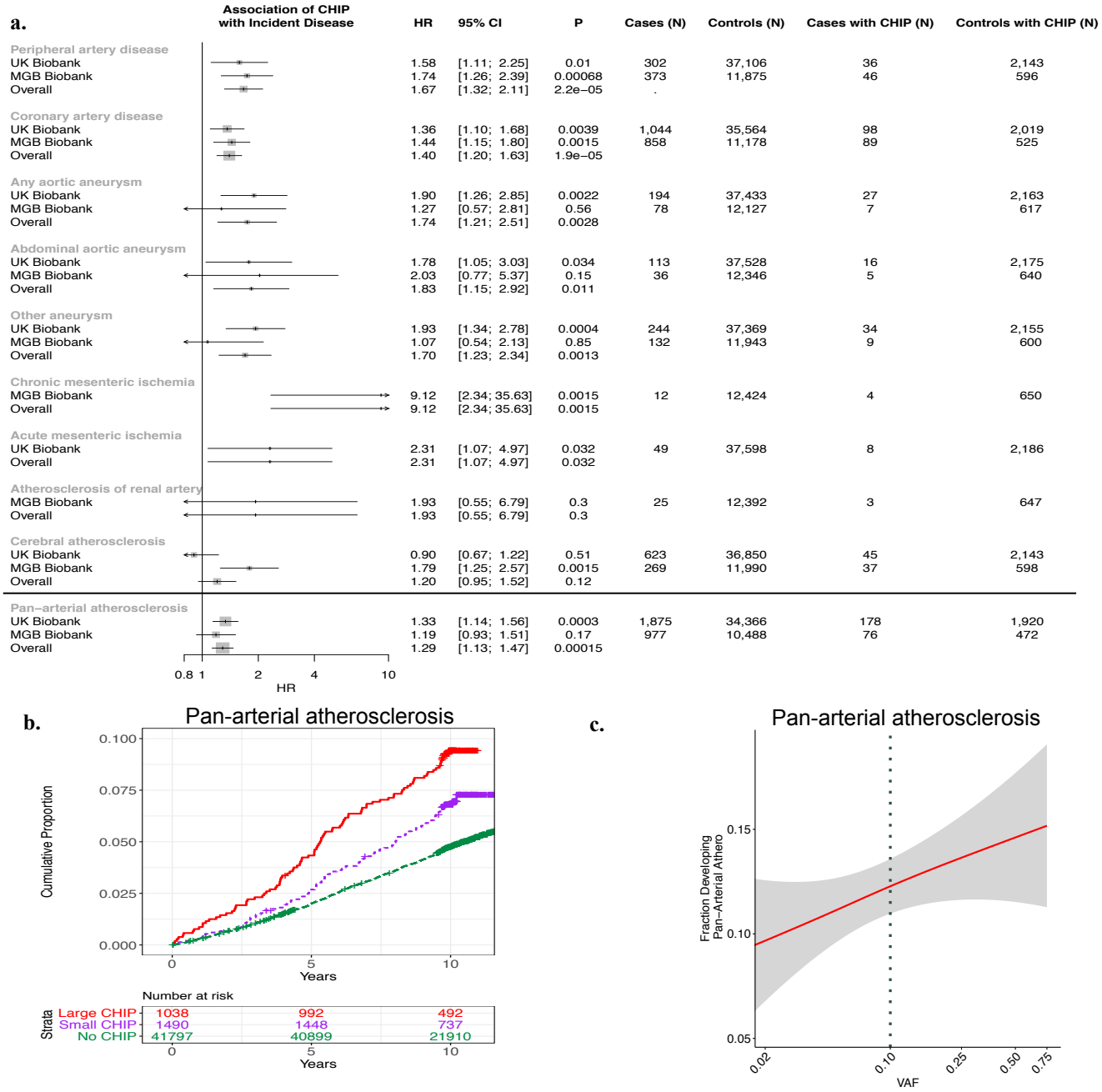

Figure 2. CHIP and incident pan-arterial atherosclerosis risk. a) Association of CHIP with 9 incident atherosclerotic diseases separately and combined in a 'Pan-arterial atherosclerosis' phenotype in the UKB, MGBB, and meta-analyzed across both studies ("Overall"). b) Cumulative risk of incident atherosclerosis across the composite 'pan-arterial atherosclerosis' phenotype stratified by no CHIP, small CHIP (VAF<10%), and large CHIP (VAF≥10%) carrier state in the UK Biobank. c) Association of CHIP VAF with fraction of individuals developing pan-arterial atherosclerosis in the UK Biobank. CHIP = clonal hematopoiesis of indeterminate potential; VAF = variant allele fraction; PAD = peripheral artery disease

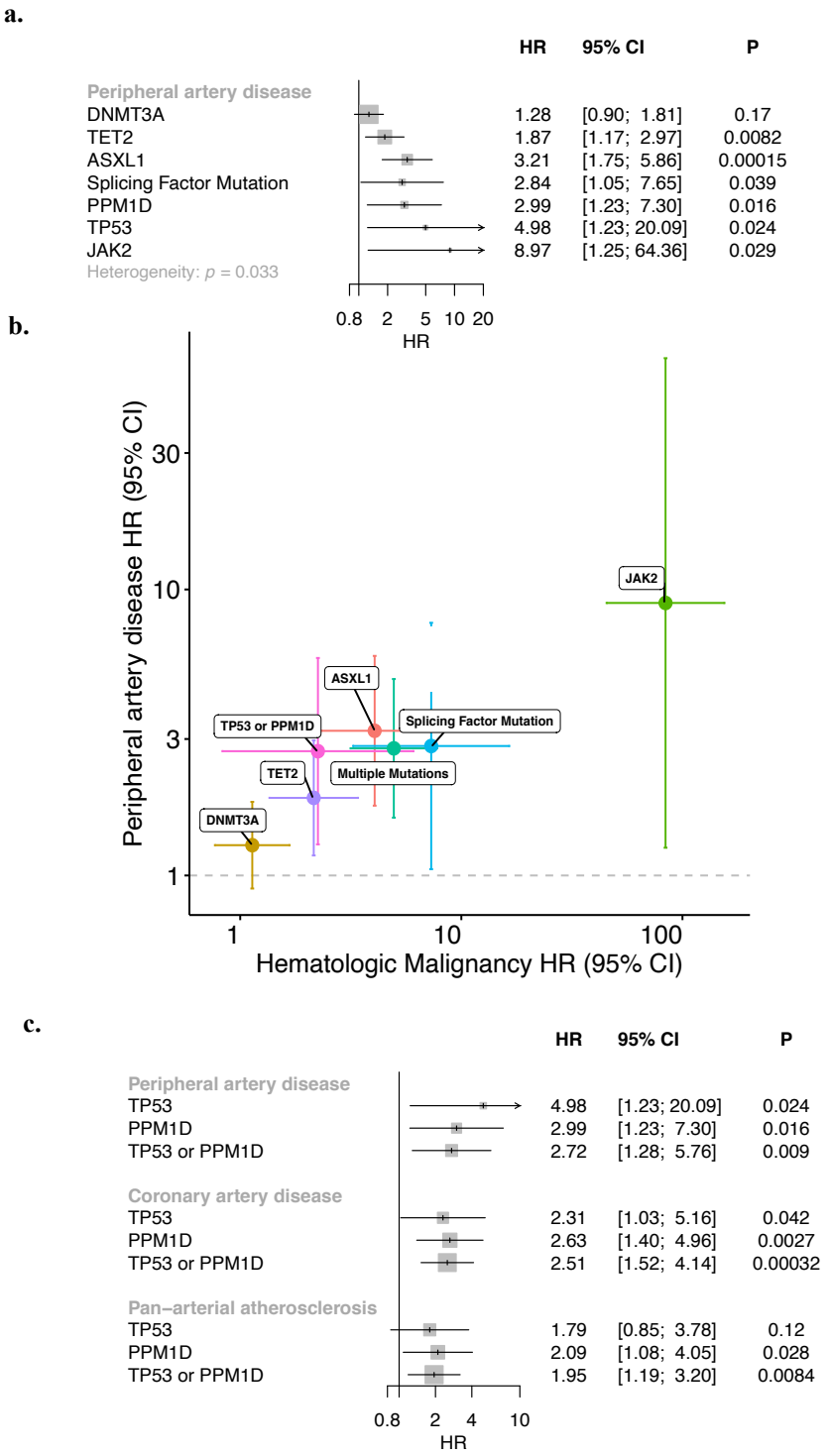

Figure 3: Gene-specific association of CHIP with incident peripheral artery disease (PAD). a) CHIP-PAD association analyses stratified by putative CHIP driver gene. Results following meta-analysis across the UKB and MGBB are shown. b) Gene-specific comparison of HR and 95% CI for hematologic malignancy (x-axis) and PAD (y-axis) in the UKB. c) Association of DDR CHIP (*PPM1D or TP53*) with incident peripheral artery disease, coronary artery disease, and pan-vascular atherosclerosis. Results across UK Biobank and MGB Biobank were combined using an inverse-variance weighted fixed effects meta-analysis. CHIP = clonal hematopoiesis of indeterminate potential; DDR = DNA-damage repair; VAF = variant allele fraction; PAD = peripheral artery disease

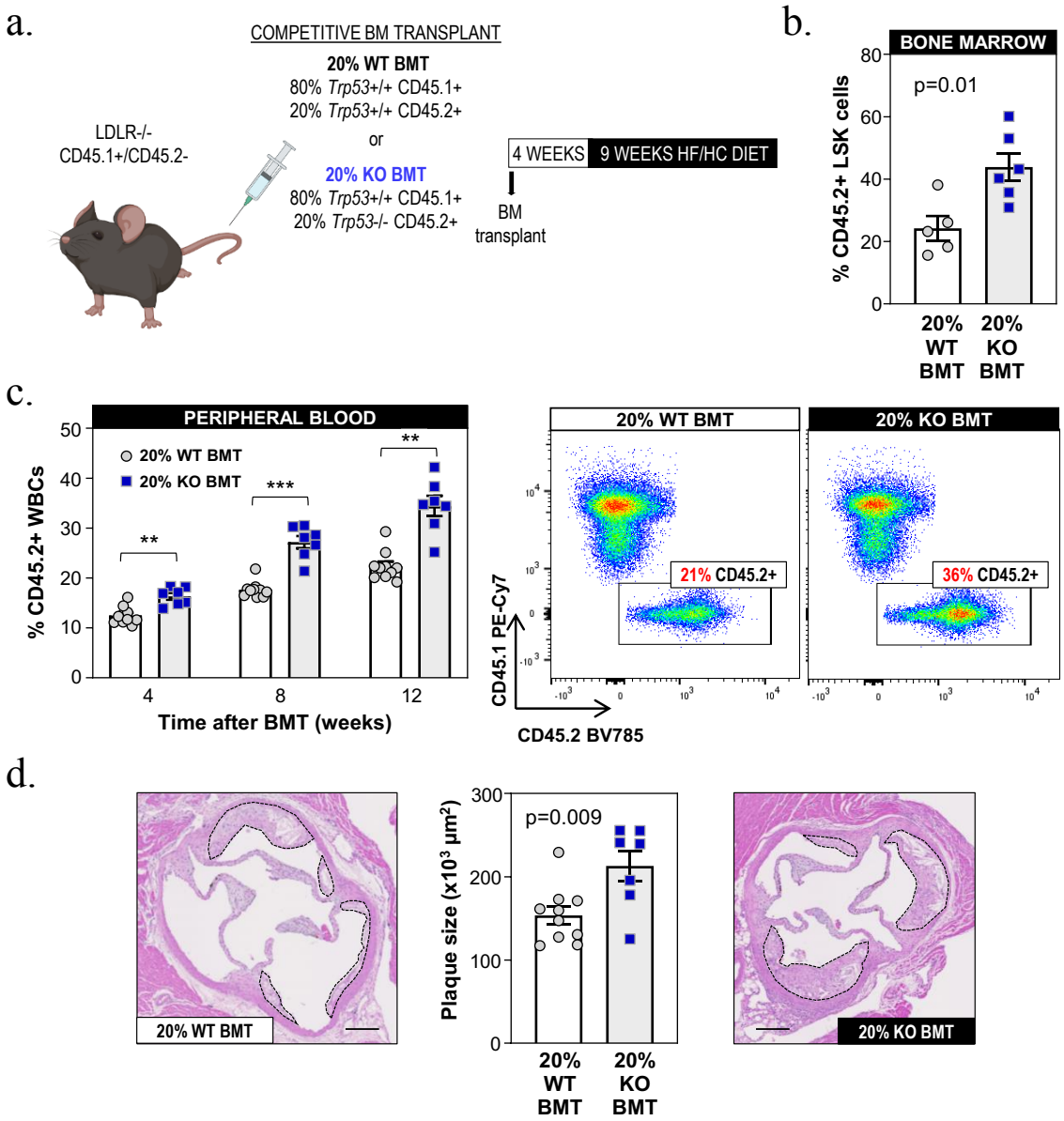

Figure 4: Accelerated atherosclerosis in a murine model of *TP53* mutation-driven CHIP. a) Summary of the competitive BMT approach and the timeline of these studies. 20% KO-BMT male mice and 20% WT-BMT controls were fed a high-fat/high-cholesterol (HF/HC) diet for 9 weeks, starting 4 weeks after BMT (n=10 20% WT-BMT, n=7 20% KO-BMT, unless otherwise noted). b) Percentage of CD45.2+ cells in the bone marrow HSPC population (Lin- Sca1+ cKit+ cells) after 9 weeks on HF/HC diet (13 weeks post-BMT), evaluated by flow cytometry (n= 5 20% WT-BMT, n=6 20% KO-BMT). c) Percentage of CD45.2+ in white blood cells, evaluated by flow cytometry (**p<0.01, ***p<0.001). Representative CD45.1/CD45.2 dot plots are shown. d) Aortic root plaque size. Representative images of hematoxylin and eosin-stained sections are shown; atherosclerotic plaques are delineated by dashed lines. Scale bars, 100 µm.

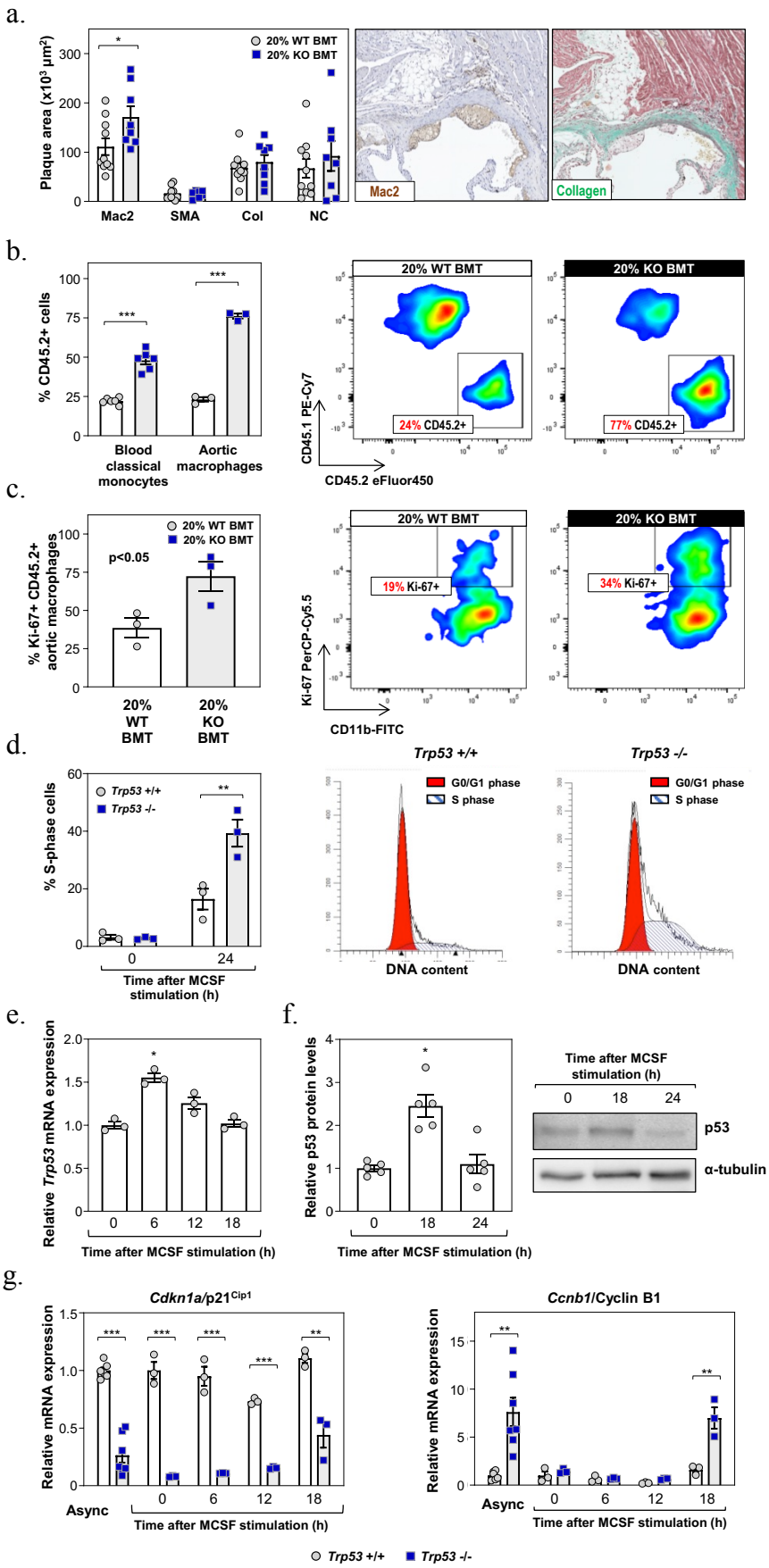
a.
Plaque area (x10³ µm²)
20% WT BMT
20% KO BMT
Mac2
SMA
Col
NC
Mac2
Collagen
b.
% CD45.2+ cells
Blood classical monocytes
Aortic macrophages
20% WT BMT
20% KO BMT
24% CD45.2+
77% CD45.2+
CD45.1 PE-Cy7
CD45.2 eFluor450
c.
% Ki-67+ CD45.2+ aortic macrophages
p<0.05
20% WT BMT
20% KO BMT
19% Ki-67+
34% Ki-67+
Ki-67 PerCP-Cy5.5
CD11b-FITC
d.
% S-phase cells
Trp53 +/+
Trp53 -/-
Time after MCSF stimulation (h)
G0/G1 phase
S phase
DNA content
e.
Relative Trp53 mRNA expression
Time after MCSF stimulation (h)
f.
Relative p53 protein levels
Time after MCSF stimulation (h)
p53
α-tubulin
g.
Cdkn1a/p21Cip1
Ccnb1/Cyclin B1
Relative mRNA expression
Async
Time after MCSF stimulation (h)
Trp53 +/+
Trp53 -/-

681

682 **Figure 5: Increased proliferation and expansion of p53-deficient macrophages.** a) Plaque
683 composition in 20% KO BMT female mice (n=10) and controls (n=8) quantified as absolute
684 intimal content of macrophages (Mac2 antigen immunostaining), vascular smooth muscle cells
685 (smooth muscle α-actin, SMA immunostaining), collagen (Masson's trichrome staining) and
686 necrotic core (collagen-free acellular regions). Representative images of Mac2- and collagen-
687 stained histological sections of 20% KO BMT mice are shown. b) Percentage of CD45.2+ cells
688 within the aortic macrophage population (CD3-, Ly6g-, CD11B+, F4/80^{Hi}, n = 3 pools of two
689 aortic arches per BM genotype) and blood classical monocytes (CD3-, CD115^{Hi}, Ly6g-, CD43^{Lo},
690 Ly6c^{Hi}, n=6 per BM genotype) of 20% KO BMT mice and controls, evaluated by flow
691 cytometry. Representative CD45.1/CD45.2 plots of aortic macrophages are shown. c) Percentage
692 of Ki-67+ proliferating cells within the aortic CD45.2+ macrophage population of 20% KO
693 BMT mice and controls (n = 3 pools of two aortic arches per BM genotype), evaluated by flow
694 cytometry. Representative plots are shown. d) % of S-phase cells in cultures of *Trp53*-/- and +/+
695 murine bone marrow-derived macrophages, evaluated by propidium iodide staining of cellular
696 DNA content and flow cytometry; treatment with MCSF was used to induce cell cycle entry and
697 progression in quiescent G0-synchronized macrophages (a representative experiment with
698 macrophages from n=3 mice per genotype is shown). e, f) qPCR (e) and Western Blot (f)
699 analyses of *Trp53* expression in cultured macrophages after MCSF mitogenic stimulation. p53
700 protein levels were normalized to α-tubulin. A representative blot is shown. g) Expression of cell
701 cycle regulators *Cdkn1a*/p21^{Cip1} and *Ccnb1*/Cyclin B1 in cultured *Trp53*-/- and +/+ macrophages
702 proliferating asynchronously (Async) or after MCSF stimulation. *p<0.05, **p<0.01,
703 ***p<0.001.

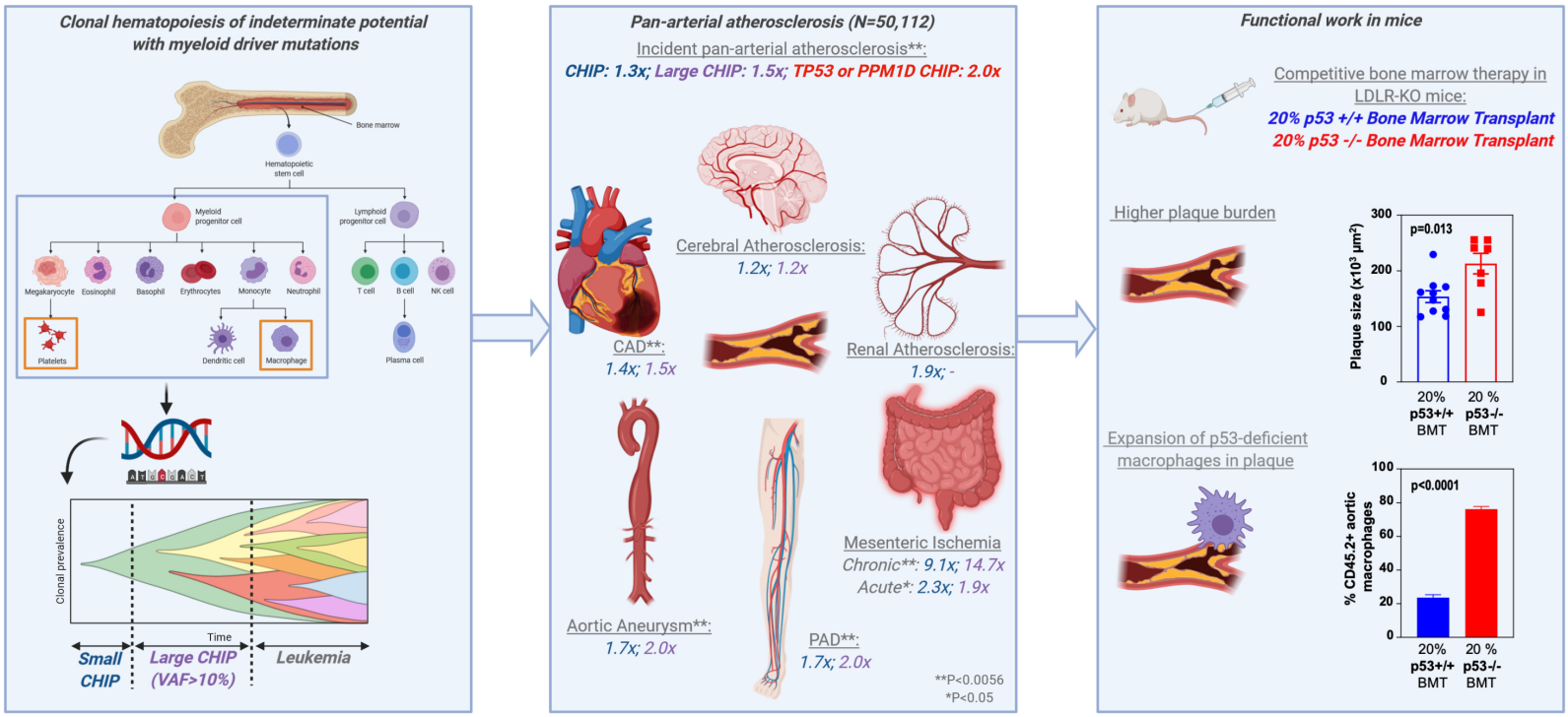

Figure 6. In this study, we assessed the association of clonal hematopoiesis of indeterminate potential (CHIP) with myeloid driver mutations with pan-arterial atherosclerosis. CHIP is a category of age-related somatic variants which are associated with incident leukemia and thought to be implicated in atherosclerosis primarily by altering macrophage function and promoting thrombosis. CHIP clones can be characterized by the fraction of blood cells carrying the clone, referred to as the variant allele fraction (VAF); here we categorized large CHIP clones as variants with VAF>10%. Across 50,112 individuals from the UK Biobank and Mass-General Brigham Biobank, we observed that CHIP is associated with increased risk of incident peripheral and pan-arterial atherosclerosis, with stronger effects conferred by large CHIP clones (HR 1.5x). In addition, we observed and a novel associations for *TP53* and *PPM1D* CHIP (HR 2.0x). CHIP was found to be individually associated with a variety of atherosclerotic conditions, with Bonferroni-significant associations (double-starred, **) identified for peripheral artery disease (PAD), coronary artery disease (CAD), aortic aneurysm, and chronic mesenteric ischemia. HR for CHIP are displayed in blue and for large CHIP in purple. Functional analysis was performed to further investigate the observed TP53-PAD association. *Ldlr*-KO 20% p53 -/- bone-marrow transplanted mice had a significant increase in plaque size, with significant expansion of p53-deficient macrophages in plaque (P<0.001) at 12 weeks.

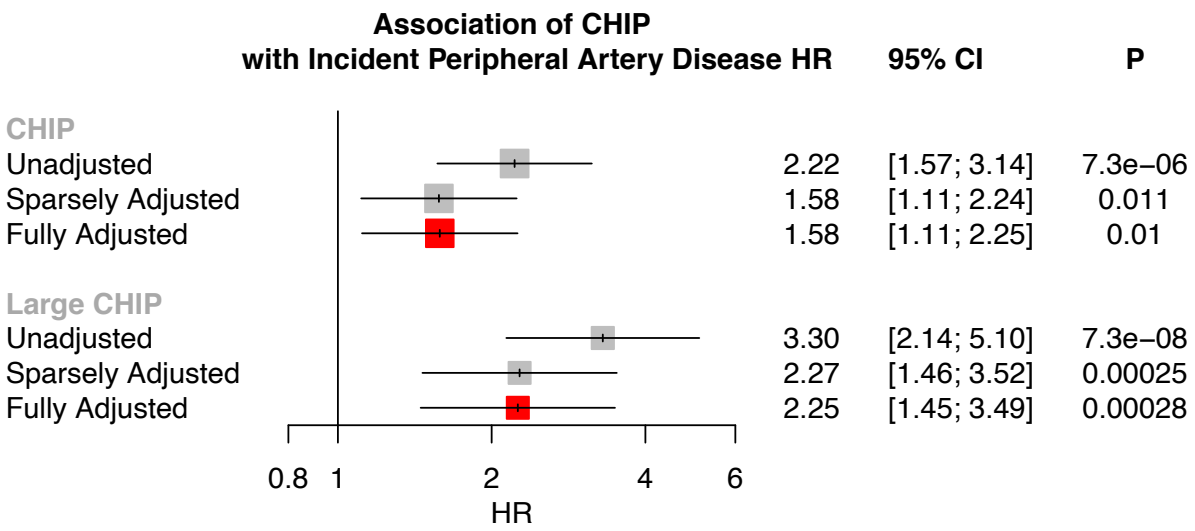

Supplementary Figure I. Association of CHIP and Large CHIP (variant allele fraction>10%) with PAD in the UKB under 1) unadjusted, 2) sparsely adjusted, and 3) fully adjusted models, where sparsely adjusted refers to the following covariates: age, age^2, sex, smoking status, Townsend deprivation index, and the first ten principal components of genetic ancestry, and the fully adjusted model additionally includes normalized BMI, prevalent hypertension, hyperlipidemia, and type 2 diabetes as covariates. Given the minimal difference between the sparsely adjusted and fully adjusted model, the sparsely adjusted model was moved forward for use in analysis.

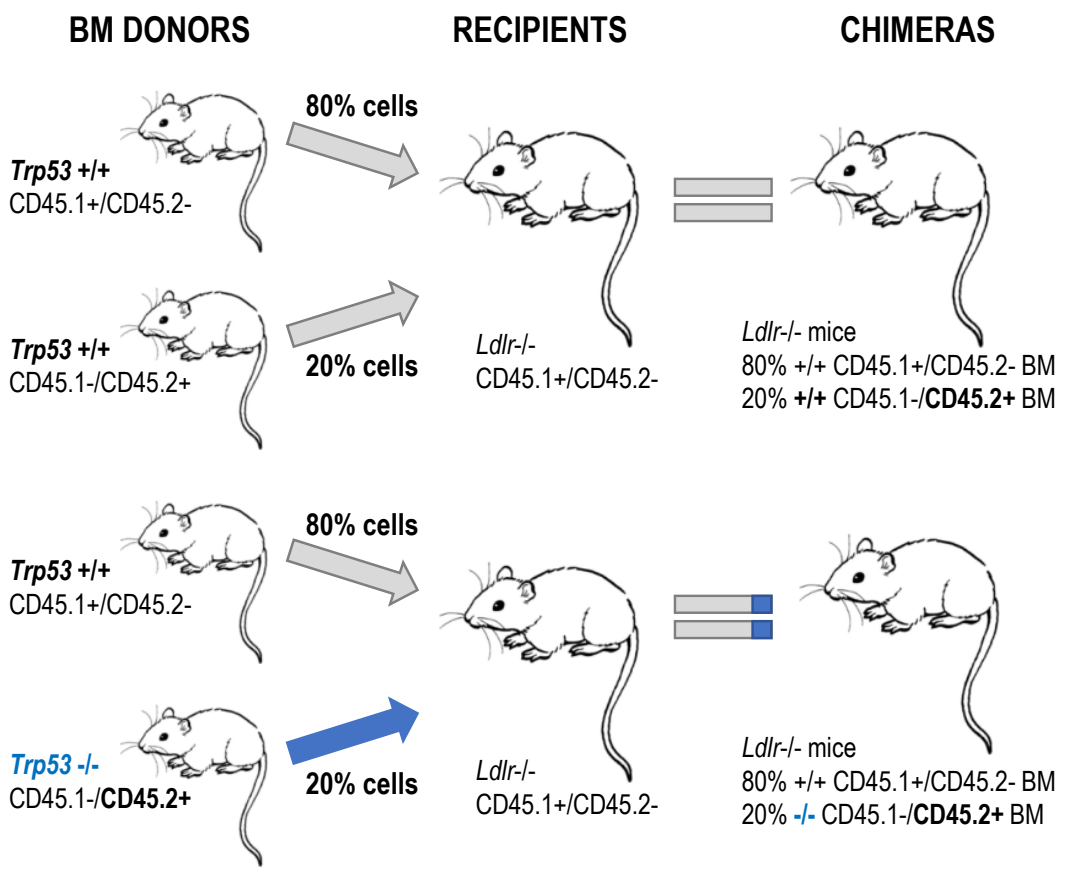

Supplementary Figure II. Competitive bone marrow transplantation approach to generate a murine model of p53 CHIP

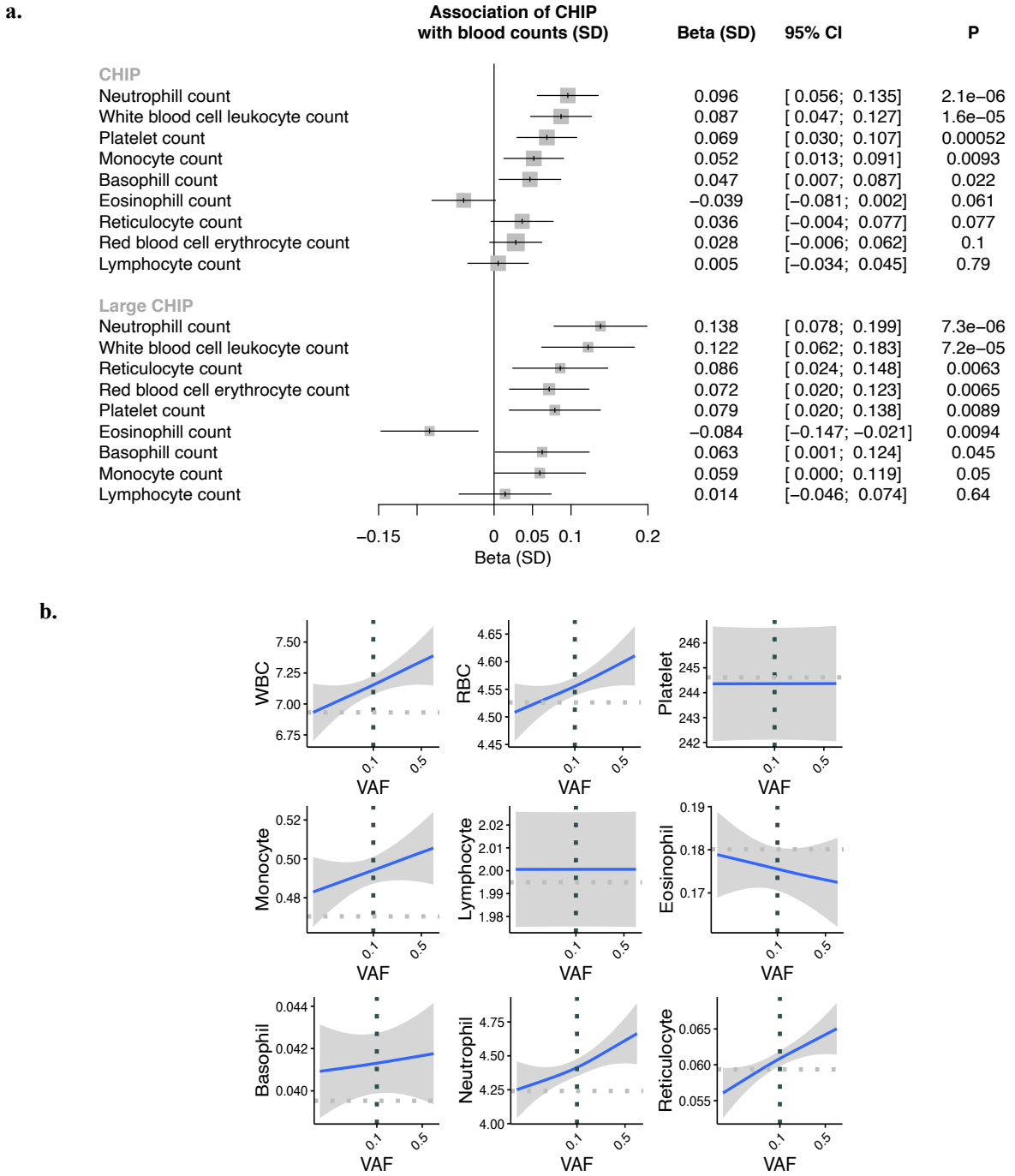

Supplementary Figure III. Association of CHIP with blood counts among individuals without prevalent hematologic malignancy in the UK Biobank. Blood counts were acquired at time of blood draw for whole exome sequencing. a) Association of CHIP and Large CHIP with normalized blood counts (SD). Associations are adjusted for age, age^2, sex, smoking status, and the first ten principal components of genetic ancestry. b) Association of CHIP variant allele frequency (VAF) with blood counts (in units of 10^9 cells/L). The gray horizontal dotted lines reflect average counts across non-CHIP carriers. The vertical black dotted line reflects the cutoff VAF for Large CHIP (VAF>0.1). CHIP = clonal hematopoiesis of indeterminate potential; VAF = variant allele fraction

a.

Association of CHIP with Incident Disease	HR	95% CI	P	Cases (N)	Controls (N)	Cases with CHIP (N)	Controls with CHIP (N)
CHIP							
Hematologic Malignancy	2.20	[1.70; 2.85]	1.8e−09	478	37,179	69	2,125
Myeloproliferative Neoplasm	5.89	[3.69; 9.39]	9.7e−14	84	37,573	27	2,167
Acute Myeloid Leukemia	8.08	[4.36; 14.97]	3.2e−11	45	37,612	17	2,177
Polycythemia Vera	12.37	[4.85; 31.54]	1.4e−07	19	37,638	8	2,186
Large CHIP							
Hematologic Malignancy	3.45	[2.54; 4.70]	3e−15	478	37,179	46	865
Myeloproliferative Neoplasm	10.62	[6.37; 17.72]	1.4e−19	84	37,573	21	890
Acute Myeloid Leukemia	9.86	[4.58; 21.24]	5e−09	45	37,612	9	902
Polycythemia Vera	22.84	[8.19; 63.72]	2.3e−09	19	37,638	6	905

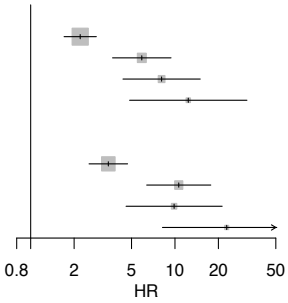

b

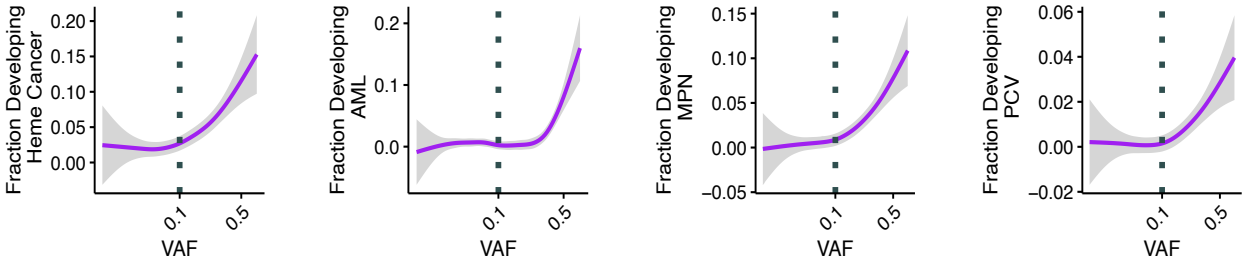

Supplementary Figure IV: Association of CHIP (a) and VAF (b) with incident hematologic malignancy among individuals without prevalent hematological malignancy in the UK Biobank. Associations are adjusted for age, age^2, sex, smoking status, Townsend deprivation index, and the first ten principal components of genetic ancestry. CHIP = clonal hematopoiesis of indeterminate potential; VAF = variant allele fraction

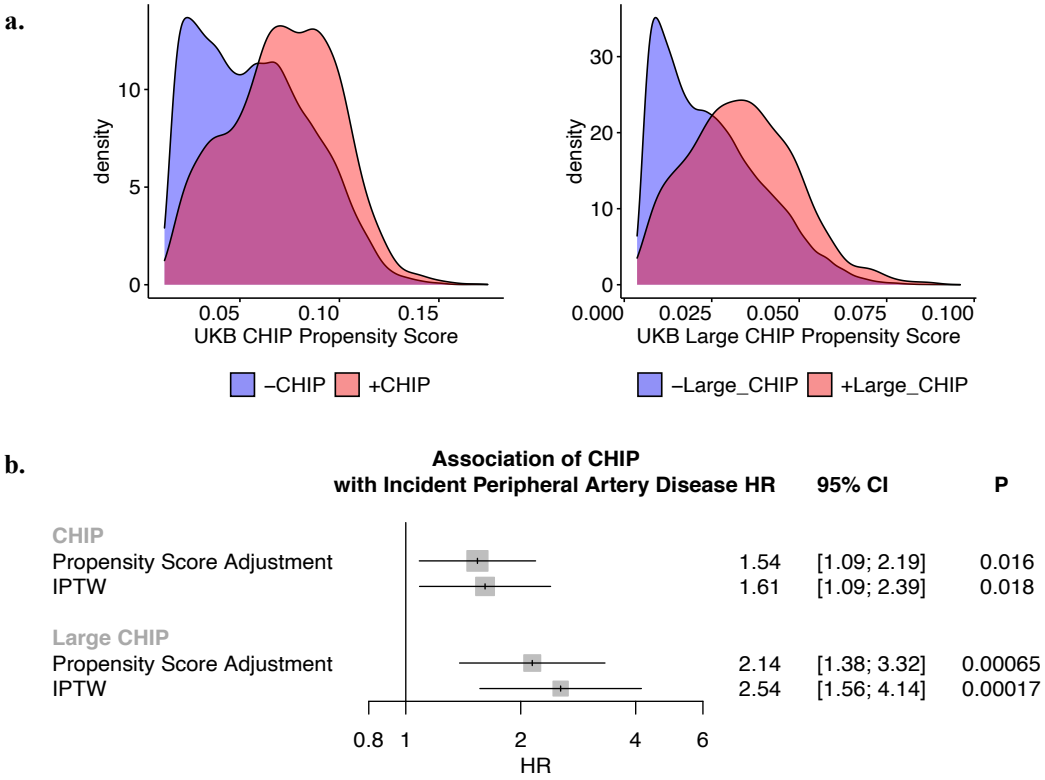

Supplementary Figure V: Epidemiological causal inference analysis for CHIP on incident peripheral artery disease in the UK Biobank. a) Propensity scores by CHIP and Large CHIP status in the UKB. **b)** Propensity score adjustment and stabilized inverse probability treatment weighting (IPTW) for the CHIP and Large CHIP association with incident PAD in the UKB. CHIP = clonal hematopoiesis of indeterminate potential; VAF = variant allele fraction; PAD = peripheral artery disease

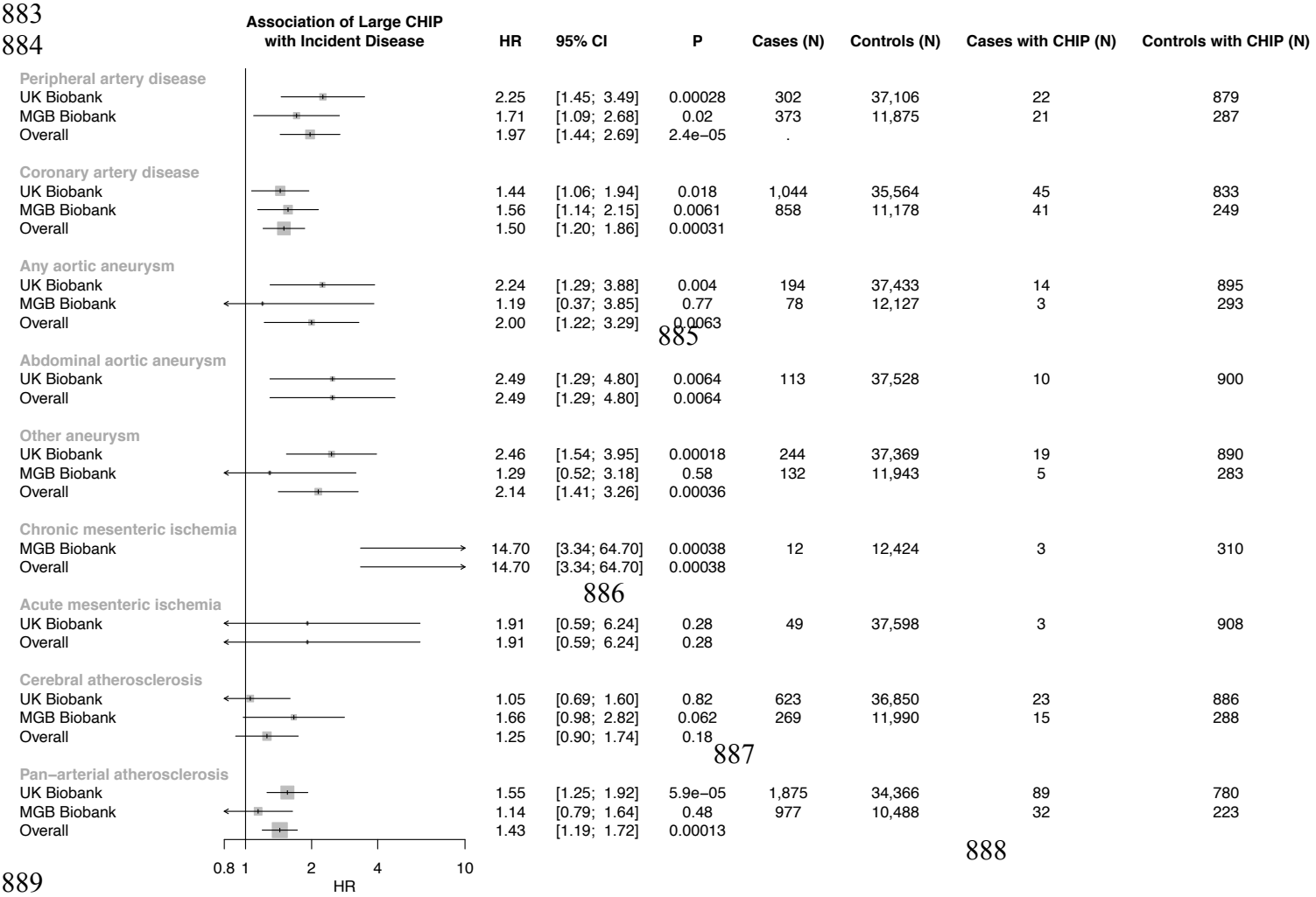

Supplementary Figure VI: Association of Large CHIP (VAF>10%) with incident pan-arterial atherosclerosis, combined across peripheral artery disease, coronary artery disease, aneurysms, chronic and acute mesenteric ischemia, cerebral atherosclerosis, and renal artery stenosis. CHIP = clonal hematopoiesis of indeterminate potential; VAF = variant allele fraction

a.

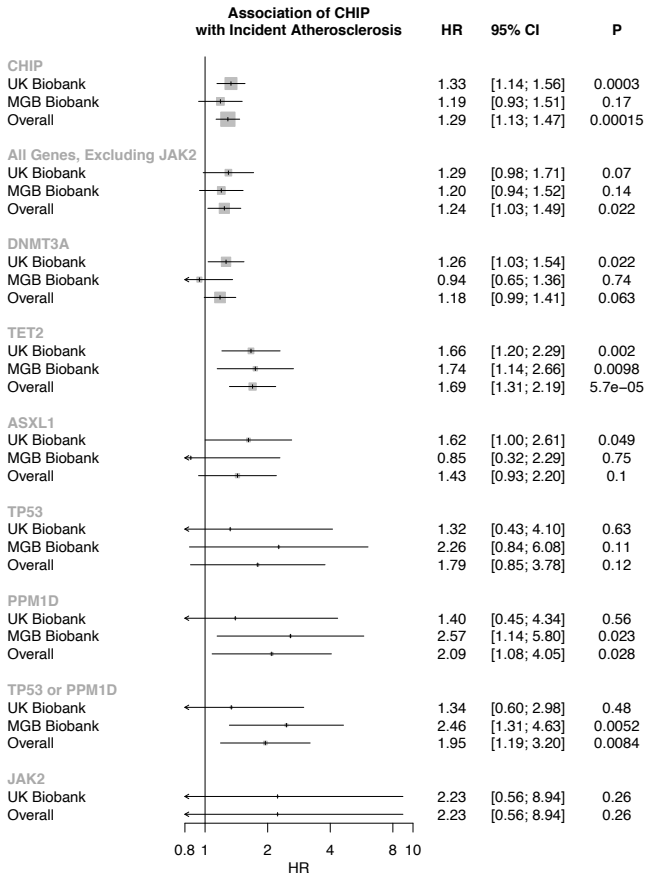

b.

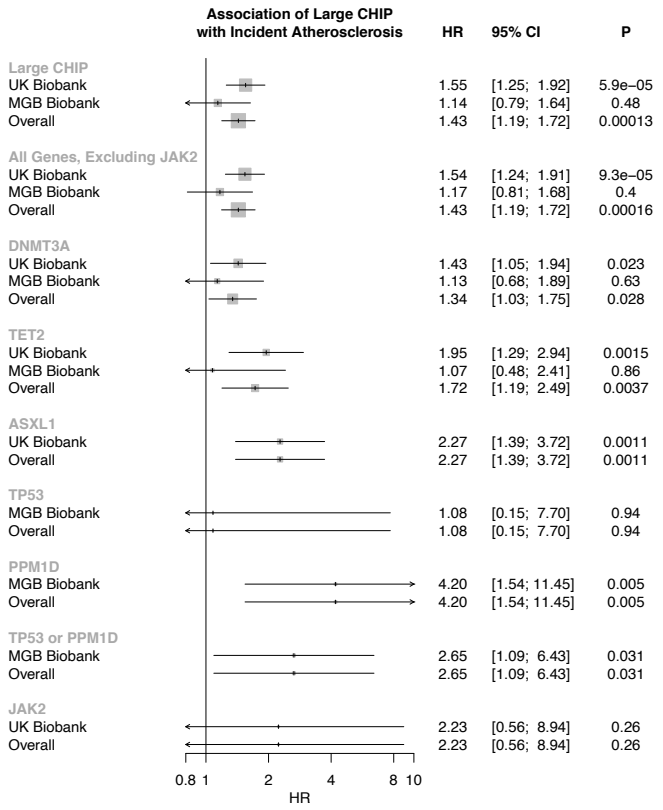

Supplementary Figure VII: Association of **a)** CHIP and **b)** Large CHIP genes with incident pan-arterial atherosclerosis, combined across peripheral artery disease, coronary artery disease, aneurysms, chronic and acute mesenteric ischemia, cerebral atherosclerosis, and renal artery stenosis. CHIP = clonal hematopoiesis of indeterminate potential; VAF = variant allele fraction

931
932

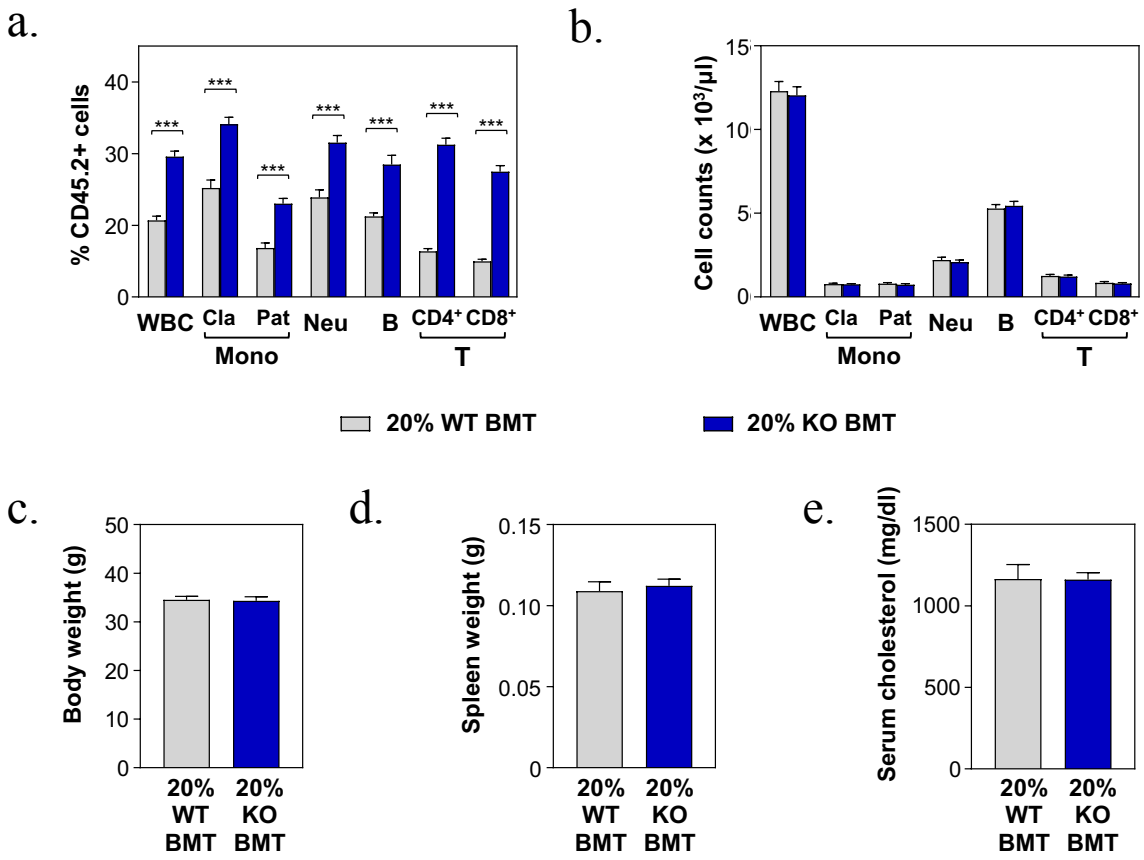

933
934

935 **Supplementary Figure VIII:** 20% KO-BMT male mice and 20% WT-BMT controls were fed a
936 high-fat/high-cholesterol (HF/HC) diet for 9 weeks, starting 4 weeks after BMT. a) Percentage of
937 CD45.2+ cells in different white blood cell (WBC) lineages in peripheral blood, evaluated by
938 flow cytometry (***p<0.001). b) Absolute counts of main WBC sub-populations in peripheral
939 blood, evaluated by flow cytometry. c) Body weight. d) Spleen weight. e) Total cholesterol level
940 in serum, evaluated by enzymatic methods.
941
942
943

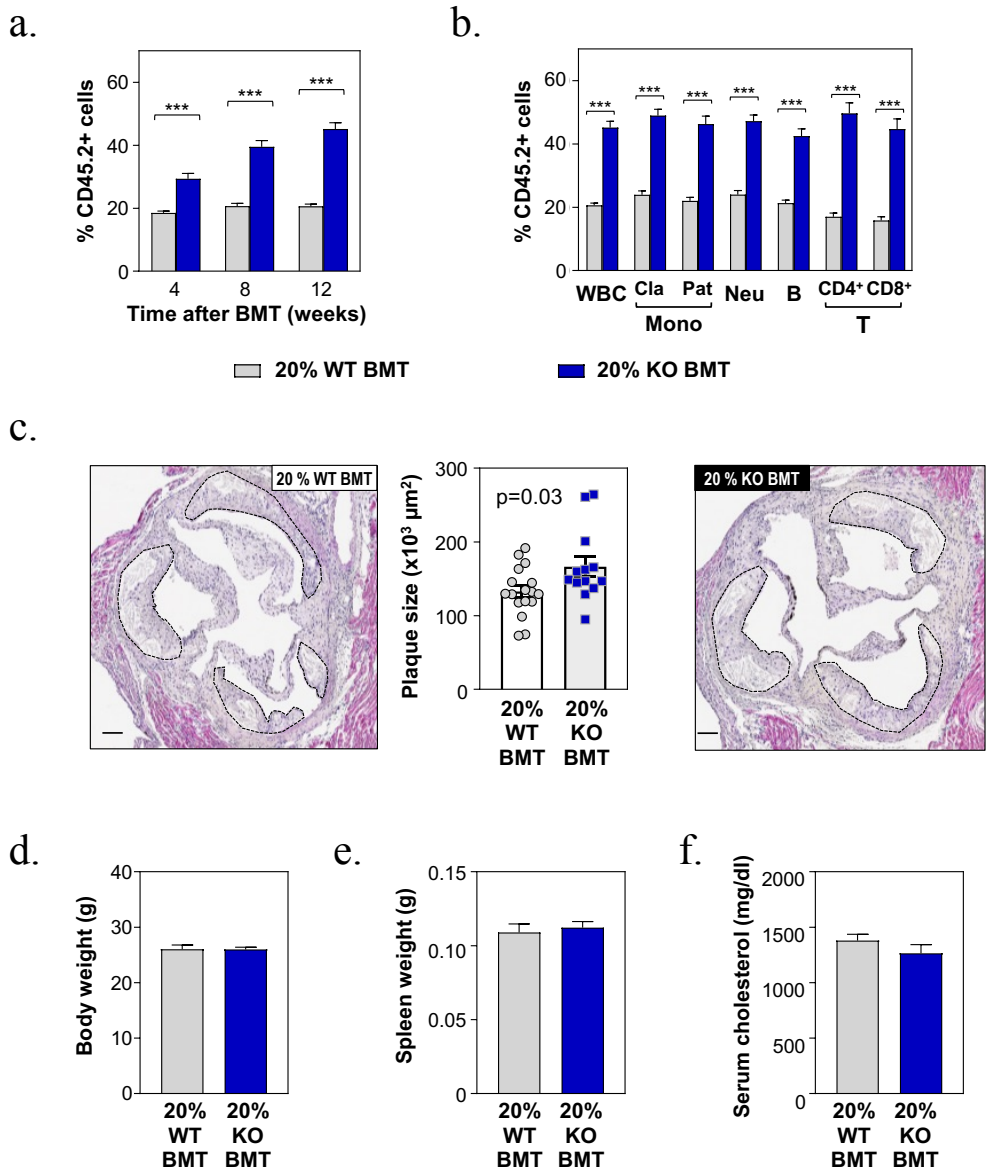

Supplementary Figure IX. 20% KO-BMT female mice (n=13) and 20% WT-BMT controls (n=17) were fed a high-fat/high-cholesterol (HF/HC) diet for 9 weeks, starting 4 weeks after BMT. a) Percentage of CD45.2+ in white blood cells at different timepoints, evaluated by flow cytometry (***p<0.001). b) Percentage of CD45.2+ cells in different white blood cell (WBC) lineages in peripheral blood after 9 weeks on HF/HC diet (13 weeks post-BMT), evaluated by flow cytometry (***p<0.001). c) Aortic root plaque size. Representative images of hematoxylin and eosin-stained sections are shown; atherosclerotic plaques are delineated by dashed lines. Scale bars, 100 µm. d) Body weight. e) Spleen weight. f) Total cholesterol level in serum, evaluated by enzymatic methods.

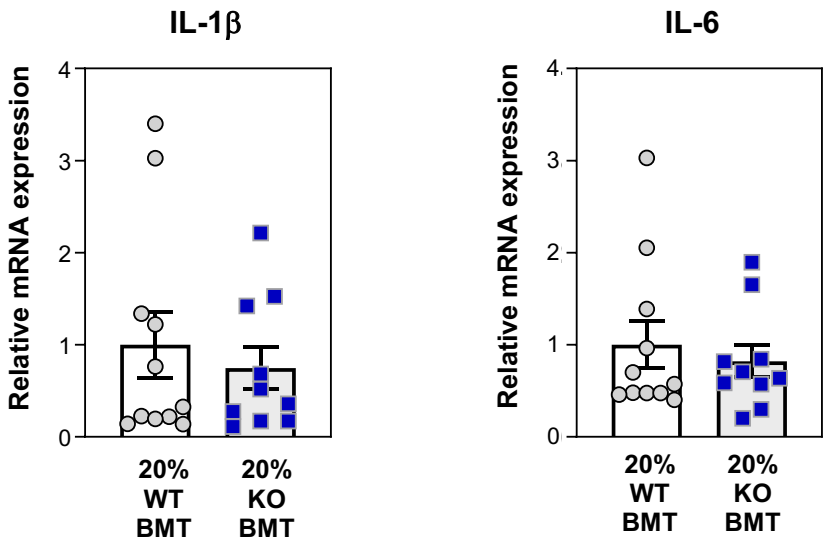

Supplementary Figure X. Aortic arch samples were obtained from HF/HC-fed 20% WT-BMT mice (n=11) or 20% KO-BMT mice (n=10) and gene expression was analyzed by qPCR analysis.

987 **Sources:**

988 1. Conte MS, Bradbury AW, Kolh P, White JV, Dick F, Fitridge R, Mills JL, Ricco JB,
989 Suresh KR and Murad MH. Global vascular guidelines on the management of chronic limb-
990 threatening ischemia. *J Vasc Surg*. 2019;69:3S-125S.e40.
991 2. Jaiswal S, Fontanillas P, Flannick J, Manning A, Grauman PV, Mar BG, Lindsley RC,
992 Mermel CH, Burtt N, Chavez A, et al. Age-Related Clonal Hematopoiesis Associated with
993 Adverse Outcomes. *New England Journal of Medicine*. 2014;371:2488-2498.
994 3. Jaiswal S, Natarajan P, Silver AJ, Gibson CJ, Bick AG, Shvartz E, McConkey M, Gupta
995 N, Gabriel S, Ardissino D, et al. Clonal Hematopoiesis and Risk of Atherosclerotic
996 Cardiovascular Disease. *New England Journal of Medicine*. 2017;377:111-121.
997 4. Xie M, Lu C, Wang J, McLellan MD, Johnson KJ, Wendl MC, McMichael JF, Schmidt
998 HK, Yellapantula V, Miller CA, et al. Age-related mutations associated with clonal
999 hematopoietic expansion and malignancies. *Nature medicine*. 2014;20:1472-8.
1000 5. Genovese G, Kähler AK, Handsaker RE, Lindberg J, Rose SA, Bakhoum SF, Chambert
1001 K, Mick E, Neale BM, Fromer M, et al. Clonal hematopoiesis and blood-cancer risk inferred
1002 from blood DNA sequence. *N Engl J Med*. 2014;371:2477-87.
1003 6. Bick AG, Pirruccello JP, Griffin GK, Gupta N, Gabriel S, Saleheen D, Libby P,
1004 Kathiresan S and Natarajan P. Genetic Interleukin 6 Signaling Deficiency Attenuates
1005 Cardiovascular Risk in Clonal Hematopoiesis. *Circulation*. 2020;141:124-131.
1006 7. Bycroft C, Freeman C, Petkova D, Band G, Elliott LT, Sharp K, Motyer A, Vukcevic D,
1007 Delaneau O, O'Connell J, et al. The UK Biobank resource with deep phenotyping and genomic
1008 data. *Nature*. 2018;562:203-209.
1009 8. Smoller JW, Karlson EW, Green RC, Kathiresan S, MacArthur DG, Talkowski ME,
1010 Murphy SN and Weiss ST. An eMERGE Clinical Center at Partners Personalized Medicine.
1011 *Journal of personalized medicine*. 2016;6.
1012 9. Van Hout CV, Tachmazidou I, Backman JD, Hoffman JD, Liu D, Pandey AK, Gonzaga-
1013 Jauregui C, Khalid S, Ye B, Banerjee N, et al. Exome sequencing and characterization of 49,960
1014 individuals in the UK Biobank. *Nature*. 2020;586:749-756.
1015 10. Bick AG, Weinstock JS, Nandakumar SK, Fulco CP, Bao EL, Zekavat SM, Szeto MD,
1016 Liao X, Leventhal MJ, Nasser J, et al. Inherited causes of clonal haematopoiesis in 97,691 whole
1017 genomes. *Nature*. 2020;586:763-768.
1018 11. Jaiswal S, Fontanillas P, Flannick J, Manning A, Grauman PV, Mar BG, Lindsley RC,
1019 Mermel CH, Burtt N, Chavez A, et al. Age-related clonal hematopoiesis associated with adverse
1020 outcomes. *N Engl J Med*. 2014;371:2488-98.
1021 12. Jaiswal S, Natarajan P, Silver AJ, Gibson CJ, Bick AG, Shvartz E, McConkey M, Gupta
1022 N, Gabriel S, Ardissino D, et al. Clonal Hematopoiesis and Risk of Atherosclerotic
1023 Cardiovascular Disease. *N Engl J Med*. 2017;377:111-121.
1024 13. Klarin D, Lynch J, Aragam K, Chaffin M, Assimes TL, Huang J, Lee KM, Shao Q,
1025 Huffman JE, Natarajan P, et al. Genome-wide association study of peripheral artery disease in
1026 the Million Veteran Program. *Nature medicine*. 2019;25:1274-1279.
1027 14. Wu P, Gifford A, Meng X, Li X, Campbell H, Varley T, Zhao J, Carroll R, Bastarache L,
1028 Denny JC, et al. Mapping ICD-10 and ICD-10-CM Codes to Phecodes: Workflow Development
1029 and Initial Evaluation. *JMIR Med Inform*. 2019;7:e14325.

1030 15. Zekavat SM, Lin S-H, Bick AG, Liu A, Paruchuri K, Uddin MM, Ye Y, Yu Z, Liu X,
1031 Kamatani Y, et al. Hematopoietic mosaic chromosomal alterations and risk for infection among
1032 767,891 individuals without blood cancer. *medRxiv*. 2020:2020.11.12.20230821.
1033 16. Hernan MA, Brumback B and Robins JM. Marginal structural models to estimate the
1034 causal effect of zidovudine on the survival of HIV-positive men. *Epidemiology*. 2000;11:561-70.
1035 17. Fuster JJ, MacLauchlan S, Zuriaga MA, Polackal MN, Ostriker AC, Chakraborty R, Wu
1036 CL, Sano S, Muralidharan S, Rius C, et al. Clonal hematopoiesis associated with TET2
1037 deficiency accelerates atherosclerosis development in mice. *Science (New York, NY)*.
1038 2017;355:842-847.
1039 18. Fuster JJ, Zuriaga MA, Zorita V, MacLauchlan S, Polackal MN, Viana-Huete V, Ferrer-
1040 Pérez A, Matesanz N, Herrero-Cervera A, Sano S, et al. TET2-Loss-of-Function-Driven Clonal
1041 Hematopoiesis Exacerbates Experimental Insulin Resistance in Aging and Obesity. *Cell reports*.
1042 2020;33:108326.
1043 19. Denny JC, Bastarache L, Ritchie MD, Carroll RJ, Zink R, Mosley JD, Field JR, Pulley
1044 JM, Ramirez AH, Bowton E, et al. Systematic comparison of phenome-wide association study of
1045 electronic medical record data and genome-wide association study data. *Nat Biotechnol*.
1046 2013;31:1102-10.
1047 20. Visconte V, M ON and H JR. Mutations in Splicing Factor Genes in Myeloid
1048 Malignancies: Significance and Impact on Clinical Features. *Cancers (Basel)*. 2019;11.
1049 21. Bondar T and Medzhitov R. p53-mediated hematopoietic stem and progenitor cell
1050 competition. *Cell Stem Cell*. 2010;6:309-22.
1051 22. Liu Y, Elf SE, Miyata Y, Sashida G, Liu Y, Huang G, Di Giandomenico S, Lee JM,
1052 Deblasio A, Menendez S, et al. p53 regulates hematopoietic stem cell quiescence. *Cell Stem Cell*.
1053 2009;4:37-48.
1054 23. TeKippe M, Harrison DE and Chen J. Expansion of hematopoietic stem cell phenotype
1055 and activity in Trp53-null mice. *Exp Hematol*. 2003;31:521-7.
1056 24. Sano S, Oshima K, Wang Y, MacLauchlan S, Katanasaka Y, Sano M, Zuriaga MA,
1057 Yoshiyama M, Goukassian D, Cooper MA, et al. Tet2-Mediated Clonal Hematopoiesis
1058 Accelerates Heart Failure Through a Mechanism Involving the IL-1beta/NLRP3 Inflammasome.
1059 *J Am Coll Cardiol*. 2018;71:875-886.
1060 25. Abplanalp WT, Cremer S, John D, Hoffmann J, Schuhmacher B, Merten M, Rieger MA,
1061 Vasa-Nicotera M, Zeiher AM and Dimmeler S. Clonal Hematopoiesis-Driver DNMT3A
1062 Mutations Alter Immune Cells in Heart Failure. *Circ Res*. 2021;128:216-228.
1063 26. Sinha SK, Miikeda A, Fouladian Z, Mehrabian M, Edillor C, Shih D, Zhou Z, Paul MK,
1064 Charugundla S, Davis RC, et al. Local M-CSF (Macrophage Colony-Stimulating Factor)
1065 Expression Regulates Macrophage Proliferation and Apoptosis in Atherosclerosis. *Arterioscler*
1066 *Thromb Vasc Biol*. 2021;41:220-233.
1067 27. Klarin D, Verma SS, Judy R, Dikilitas O, Wolford BN, Paranjpe I, Levin MG, Pan C,
1068 Tcheandjieu C, Spin JM, et al. Genetic Architecture of Abdominal Aortic Aneurysm in the
1069 Million Veteran Program. *Circulation*. 2020.
1070 28. Shimizu K, Mitchell RN and Libby P. Inflammation and cellular immune responses in
1071 abdominal aortic aneurysms. *Arterioscler Thromb Vasc Biol*. 2006;26:987-94.
1072 29. Boesten LS, Zadelaar AS, van Nieuwkoop A, Hu L, Teunisse AF, Jochemsen AG, Evers
1073 B, van de Water B, Gijbels MJ, van Vlijmen BJ, et al. Macrophage p53 controls macrophage
1074 death in atherosclerotic lesions of apolipoprotein E deficient mice. *Atherosclerosis*.
1075 2009;207:399-404.

1076 30. Fuster JJ, Fernandez P, Gonzalez-Navarro H, Silvestre C, Nabah YN and Andres V.
1077 Control of cell proliferation in atherosclerosis: insights from animal models and human studies.
1078 *Cardiovasc Res*. 2010;86:254-64.
1079 31. Guevara NV, Kim HS, Antonova EI and Chan L. The absence of p53 accelerates
1080 atherosclerosis by increasing cell proliferation in vivo. *Nat Med*. 1999;5:335-9.
1081 32. Mercer J, Figg N, Stoneman V, Braganza D and Bennett MR. Endogenous p53 protects
1082 vascular smooth muscle cells from apoptosis and reduces atherosclerosis in ApoE knockout
1083 mice. *Circ Res*. 2005;96:667-74.
1084 33. Merched AJ, Williams E and Chan L. Macrophage-specific p53 expression plays a
1085 crucial role in atherosclerosis development and plaque remodeling. *Arterioscler Thromb Vasc*
1086 *Biol*. 2003;23:1608-14.
1087 34. Sanz-Gonzalez SM, Barquin L, Garcia-Cao I, Roque M, Gonzalez JM, Fuster JJ, Castells
1088 MT, Flores JM, Serrano M and Andres V. Increased p53 gene dosage reduces neointimal
1089 thickening induced by mechanical injury but has no effect on native atherosclerosis. *Cardiovasc*
1090 *Res*. 2007;75:803-12.
1091 35. van Vlijmen BJ, Gerritsen G, Franken AL, Boesten LS, Kockx MM, Gijbels MJ,
1092 Vierboom MP, van Eck M, van De Water B, van Berkel TJ, et al. Macrophage p53 deficiency
1093 leads to enhanced atherosclerosis in APOE*3-Leiden transgenic mice. *Circ Res*. 2001;88:780-6.
1094 36. Robbins CS, Hilgendorf I, Weber GF, Theurl I, Iwamoto Y, Figueiredo JL, Gorbatov R,
1095 Sukhova GK, Gerhardt LM, Smyth D, et al. Local proliferation dominates lesional macrophage
1096 accumulation in atherosclerosis. *Nat Med*. 2013;19:1166-72.
1097 37. Heyde A, Rohde D, McAlpine CS, Zhang S, Hoyer FF, Gerold JM, Cheek D, Iwamoto
1098 Y, Schloss MJ, Vandoorne K, et al. Increased stem cell proliferation in atherosclerosis
1099 accelerates clonal hematopoiesis. *Cell*. 2021;184:1348-1361 e22.
1100 38. Fidler TP, Xue C, Yalcinkaya M, Hardaway B, Abramowicz S, Xiao T, Liu W, Thomas
1101 DG, Hajebrahimi MA, Pircher J, et al. The AIM2 inflammasome exacerbates atherosclerosis in
1102 clonal haematopoiesis. *Nature*. 2021;592:296-301.
1103